

IFJPAN-IV-2011-6 UAB-FT/695  
FTUV/2011-0929 IFIC/11-53 CERN-PH-TH/2012-016

# Resonance chiral Lagrangian currents and $\tau$ decay Monte Carlo

O. Shekhovtsova<sup>a</sup>, T. Przedziński<sup>b</sup>, P. Roig<sup>c</sup> and Z. Was<sup>d,e</sup>

<sup>a</sup>*IFIC, Universitat de València-CSIC, Apt. Correus 22085,  
E-46071, València, Spain*

<sup>b</sup>*The Faculty of Physics, Astronomy and Applied Computer Science,  
Jagellonian University, Reymonta 4, 30-059 Cracow, Poland*

<sup>c</sup>*Grup de Física Teòrica, Institut de Física d'Altes Energies, Universitat Autònoma de  
Barcelona, E-08193 Bellaterra, Barcelona, Spain*

<sup>d</sup>*Institute of Nuclear Physics, PAN, Kraków, ul. Radzikowskiego 152, Poland*

<sup>e</sup>*CERN PH-TH, CH-1211 Geneva 23, Switzerland*

## ABSTRACT

In the present paper we describe the set of form factors for hadronic  $\tau$  decays based on **Resonance Chiral Theory**. The technical implementation of the form factors in FORTRAN code is also explained. It is shown how it can be installed into TAUOLA Monte Carlo program. Then it is rather easy to implement into software environments of not only Belle and BaBar collaborations but also for FORTRAN and C++ applications of LHC. The description of the current for each  $\tau$  decay mode is complemented with technical numerical tests. The set is ready for fits, parameters to be used in fits are explained. Arrangements to work with the experimental data not requiring unfolding are prepared. Hadronic currents, ready for confrontation with the  $\tau$  decay data, but not yet ready for the general use, cover more than 88 % of hadronic  $\tau$  decay width.

IFJPAN-IV-2011-6 UAB-FT/695 FTUV/2011-09-29 IFIC/11-53  
CERN-PH-TH/2012-016  
March, 2012

# Contents

<b>1</b>	<b>Introduction</b>	<b>3</b>
<b>2</b>	<b>Hadronic current for two and three hadrons</b>	<b>5</b>
2.1	$\pi^-\pi^-\pi^+\nu_\tau$ and $\pi^0\pi^0\pi^-\nu_\tau$ . . . . .	7
2.2	$K^-\pi^-K^+\nu_\tau$ and $K^0\pi^-\bar{K}^0\nu_\tau$ . . . . .	9
2.3	$K^-\pi^0K^0\nu_\tau$ . . . . .	11
2.4	$\pi^-\pi^0\nu_\tau$ , $\pi^0K^-\nu_\tau$ , $\pi^-\bar{K}^0\nu_\tau$ and $K^-K^0\nu_\tau$ . . . . .	12
<b>3</b>	<b>Energy-dependent widths of resonances</b>	<b>14</b>
<b>4</b>	<b>Benchmark calculations for three-pion mode</b>	<b>17</b>
4.1	Technical test . . . . .	17
4.2	Test with semirealistic parameters . . . . .	18
<b>5</b>	<b>Numerical results for two and three-pseudoscalar channels</b>	<b>20</b>
5.1	$\pi^-\pi^-\pi^+\nu_\tau$ and $\pi^0\pi^0\pi^-\nu_\tau$ . . . . .	21
5.2	$K^-\pi^-K^+\nu_\tau$ and $K^0\pi^-\bar{K}^0\nu_\tau$ . . . . .	22
5.3	$K^-\pi^0K^0\nu_\tau$ . . . . .	23
5.4	$\pi^-\pi^0\nu_\tau$ , $\pi^0K^-\nu_\tau$ , $\pi^-\bar{K}^0\nu_\tau$ and $K^-K^0\nu_\tau$ . . . . .	24
5.5	Attempt at comparison with the data . . . . .	25
<b>6</b>	<b>Program organization</b>	<b>27</b>
6.1	Weight recalculation . . . . .	27
<b>7</b>	<b>Theoretical basis of the currents</b>	<b>29</b>
7.1	Resonance Chiral Theory framework . . . . .	29
7.2	The error associated to the $1/N_C$ expansion . . . . .	31
7.3	Other sources of error . . . . .	32
7.4	Numerical estimates of the errors in the different decay channels and distributions . . . . .	33
<b>8</b>	<b>Summary</b>	<b>34</b>
<b>A</b>	<b>Useful functions and notations</b>	<b>43</b>
<b>B</b>	<b>Installation</b>	<b>44</b>
B.1	Changes for host TAUOLA version . . . . .	45
B.2	Calculating numerical tables used by form factors . . . . .	47
B.2.1	Executing the code . . . . .	47
B.2.2	Setup . . . . .	47
B.3	Tests . . . . .	47
B.3.1	Numerical stability tests . . . . .	48

B.3.2	Analytic integration test . . . . .	49
B.4	TAUOLA weight recalculation mode . . . . .	50
B.4.1	Weight recalculation algorithm . . . . .	50
B.5	TAUOLA++ installation . . . . .	51
<b>C</b>	<b>Input parameters</b>	<b>51</b>
C.1	Range of variation of the non-resonance input parameters . . . . .	53
C.2	Range of variation of the resonance input parameters . . . . .	53
<b>D</b>	<b>Benchmark results</b>	<b>55</b>
<b>E</b>	<b>Final state interactions</b>	<b>55</b>

# 1 Introduction

Measurements of  $\tau$  lepton, because of its long lifetime, large mass and parity sensitive couplings, lead to broad physics interest. From the perspective of high-energy experiments such as at LHC, knowledge of  $\tau$  lepton properties offers an important ingredient of new physics signatures. From the perspective of lower energies,  $\tau$  lepton decays constitute an excellent laboratory for hadronic interactions. In itself, the  $\tau$  lepton decays constitute an excellent laboratory for studies of hadronic interactions at the energy scale of about 1 GeV, where neither perturbative QCD methods nor chiral Lagrangians are expected to work to a good precision [1, 2, 3, 4, 5]. At present, hundreds of millions of  $\tau$  decays are amassed by both Belle and BaBar experiments. It is of utmost importance to represent such data in a form as useful for general applications as possible.

Most of these data samples are not yet analyzed. For example, in Ref. [6] only 10 % of the collected sample, which means 5.4 M events for  $\tau^\pm \rightarrow \nu_\tau \pi^\pm \pi^0$ , was used. Future samples at the Belle II or Frascati Super B facilities will be even larger [7, 8]. That means that already now the statistical error for the collected samples of  $\tau \rightarrow 3\pi\nu_\tau$  is of the order of 0.03 %. For  $\tau \rightarrow K\pi\nu_\tau$  it is about 0.1 % and for  $\tau \rightarrow KK\pi\nu_\tau$  at the level of 0.2 %. To exploit such valuable data sets, theoretical predictions need to be properly prepared. As typically several millions of events per channel are collected, that means that the statistical error can reach  $\sim 0.03$  %. To match it, parametrizations of hadronic currents resulting from theoretical models must be controlled to technical precision better than 0.03 % in Monte Carlo, combining theoretical aspects and full detector response. Only then, one can be sure that the comparison of the data with theoretical predictions exploits in full the statistical impact of the data, and one can concentrate on systematic effects both for theory and experiment. One should stress that the above technical precision is required not only for signal distribution, but for background as well. Sophisticated techniques allowing proper comparisons of the data and models are also needed.

A review of the status of available tools for such studies of  $\tau$  decays can be found in Ref. [9]. It was concluded in Ref. [9] that the appropriate choice of hadronic current parametrization was the most essential missing step to perform. It was also found that, for the decays involving more than two pseudoscalars in the final state, the appropriate use of hadronic currents in fits is important too. At present, standards of precision are at 2 % level. This is a factor of 100 less than what is required. For many  $\tau$  decay modes even this 2 % precision level is far to be reached [10].

The original version of TAUOLA [11] uses the results of Ref. [12, 13] and their extensions to other decay channels<sup>1</sup>. In that model each three-pseudoscalar current is constructed as a weighed sum of products of Breit-Wigner functions [5, 12, 15, 16]. This approach was contested in Ref. [17] where it was demonstrated that the corresponding hadronic form factors, which were written to reproduce the leading-order (LO)  $\chi PT$  result [18], fail to reproduce the next-to-leading-order one (NLO) [19, 20]. The corresponding parametrization based

---

<sup>1</sup>With time, due to pressure from the experimental community, many other parametrizations were introduced, but not in a systematic way. Some of those found its way to TAUOLA later, Ref. [14], and are used as a starting reference point for our present project as seen from the computing side.

on Breit-Wigner functions was not able to reproduce CLEO  $\tau^- \rightarrow (KK\pi)^-\nu_\tau$  decays data [21]. This resulted in the CLEO collaboration reshaping the model by the introduction of two ad-hoc parameters that spoil the QCD normalization of the Wess-Zumino part. This shows that, although the approach of weighted products of Breit-Wigner functions was sufficient and very successful twenty years ago now, with the massively increased experimental data samples, it is pressing to upgrade. As an alternative, an approach based on the Resonance Chiral Theory [22, 23] was proposed. Its application to hadronic tau decays is supposed to be consistent and theoretically well founded (see Sect. 7 for the related discussion). However, its results have to be confronted with the experimental data before actual improvement will be confirmed. The hadronic currents for the two and three pseudoscalar final states that we consider here have been calculated in the framework of R $\chi$ T [17, 24, 25, 26, 27] and have been prepared for TAUOLA.

Section 2 is devoted to a general presentation of the form hadronic currents must fulfil to be installed into TAUOLA generator [11]. In each subsection analytic forms of currents calculated within Resonance Chiral Theory are given channel by channel. In Section 3 energy-dependent widths as used in the parametrization of intermediate resonances are presented. Section 4 is dedicated to technical tests of the channel  $\tau \rightarrow 3\pi\nu_\tau$ . For channels involving kaons, only overall benchmark distributions are collected. The details of technical tests are left to the project Web page [28]. For all decay channels numerical results, which are of more physical interest, are collected in Section 5. Within it, the three-meson channels, which have been worked out in more depth, are first presented and then, the two meson channels are discussed. In both cases technical aspects are worked out to precision better than 0.1 %.

The organization of the hadronic currents and how they can be integrated into the TAUOLA library is explained in Section 6 and in Appendix B. Section 7 is prepared for a reader who is oriented towards the theoretical details of calculation and estimation of theoretical uncertainties of the approach. It provides arguments necessary for discussion of the range of parameters allowed for fits. The summary in Section 8 closes the paper. Further technical appendices are also given. Appendix A lists analytic functions used in the parametrization of hadronic currents. Appendix C provides numerical values of the model parameters used all over the paper. It is explained which parameters and in which range can be modified without breaking assumptions of the model and where in the code they are defined. Appendix D collects branching ratios of the newly prepared  $\tau$  decay channels as calculated by Monte Carlo simulation. It contains explicit references to the definition of the hadronic current in each decay channel, which are spread all over the paper. In the future, however, these definitions can be replaced by the new references.

The implementation of final state interactions (FSI) in the two-meson  $\tau$  decay modes is discussed in Appendix E. An improvement of the latter and the scalar form factor in  $\tau \rightarrow K\pi\nu_\tau$  decays will be addressed in a forthcoming publication [29].

Finally let us stress that our paper aims at explaining how this new set of hadronic currents can be installed in TAUOLA, independently of whether it is a standalone version, part of Belle/BaBar software or a different configuration, which is another purpose of Appendix B.

## 2 Hadronic current for two and three hadrons

Before discussing in detail the implementation of the currents into the program and resulting distributions, let us first collect here all necessary formulas. In general we will follow conventions for normalizations as used in Ref. [11]. We will not recall here relations between hadronic distributions and decay product distributions though. They are rather simple and we assume that the reader is familiar with the necessary parts of Ref. [11]. Let us recall the matrix element  $\mathcal{M}$  for the  $\tau$  decay into hadronic state  $X$  and a neutrino:  $\tau(P) \rightarrow X\nu_\tau(N)$ . It reads  $\mathcal{M} = \frac{G_F}{\sqrt{2}}\bar{u}(N)\gamma^\mu(1-\gamma_5)u(P)J_\mu$ . All dynamics of hadronic interactions is encapsulated in a current  $J_\mu$ , which is a function of hadronic  $\tau$  decay products only.

Contrary to TAUOLA, as documented in Refs. [11] or [14], now hadronic currents for all two-pseudoscalar final states are defined in separate routines and the constraint that the scalar form factor must be set to 0 is removed.

For  $\tau$  decay channels with two mesons [ $h_1(p_1)$  and  $h_2(p_2)$ ], the hadronic current reads

$$J^\mu = N \left[ \left( p_1 - p_2 - \frac{\Delta_{12}}{s}(p_1 + p_2) \right)^\mu F^V(s) + \frac{\Delta_{12}}{s}(p_1 + p_2)^\mu F^P(s) \right], \quad (1)$$

where  $s = (p_1 + p_2)^2$  and  $\Delta_{12} = m_1^2 - m_2^2$ . The formulas for vector,  $F^V(s)$ , and pseudoscalar,  $F^P(s)$ , form factors depend on the particular decay channel<sup>2</sup> and are given, respectively, for the  $\pi^-\pi^0$ ,  $(K\pi)^-$  and  $K^-K^0$  decay modes in subsection 2.4 and the following ones<sup>3</sup>.  $SU(3)$  symmetry relates all four normalization factors by the appropriate Clebsch-Gordan coefficient:

$$N^{\pi^-\pi^0} = 1, \quad N^{K^-K^0} = \frac{1}{\sqrt{2}}, \quad N^{\pi^-\bar{K}^0} = \frac{1}{\sqrt{2}}, \quad N^{\pi^0K^-} = \frac{1}{2}. \quad (2)$$

For the final state of three pseudoscalars, with momenta  $p_1$ ,  $p_2$  and  $p_3$ , Lorentz invariance determines the decomposition of the hadronic current to be

$$J^\mu = N \left\{ T_\nu^\mu \left[ c_1(p_2 - p_3)^\nu F_1 + c_2(p_3 - p_1)^\nu F_2 + c_3(p_1 - p_2)^\nu F_3 \right] + c_4 q^\mu F_4 - \frac{i}{4\pi^2 F^2} c_5 \epsilon^{\mu\nu\rho\sigma} p_1^\nu p_2^\rho p_3^\sigma F_5 \right\}, \quad (3)$$

where  $T_{\mu\nu} = g_{\mu\nu} - q_\mu q_\nu / q^2$  denotes the transverse projector, and  $q^\mu = (p_1 + p_2 + p_3)^\mu$  is the momentum of the hadronic system. The decay products are ordered and their four-momenta are denoted, respectively, as  $p_1$ ,  $p_2$  and  $p_3$ . Here and afterward in the paper  $F$  stands for the pion decay constant in the chiral limit.

Functions  $F_i$  (hadronic form factors) depend in general on three independent invariant masses that can be constructed from the three meson four-vectors. We chose  $q^2 = (p_1 +$

---

<sup>2</sup>The vector form factor of both two pions and two kaons is expected to be fixed at zero momentum transfer by gauge invariance in the  $SU(2)$  symmetry limit [30]:  $F^V(0) = 1$ , see Section 2.4.

<sup>3</sup>Two-meson  $\tau$  decays involving an  $\eta$  meson,  $\tau \rightarrow \eta^{(\prime)} P^- \nu_\tau$ ,  $P = \pi, K$  have a negligible branching fraction [31, 32].

$p_2 + p_3)^2$  and two invariant masses  $s_1 = (p_2 + p_3)^2$ ,  $s_2 = (p_1 + p_3)^2$  built from pairs of momenta. Then  $s_3 = (p_1 + p_2)^2$  can be calculated from the other three invariants,  $s_3 = q^2 - s_1 - s_2 + m_1^2 + m_2^2 + m_3^2$ , and  $F_i$  written explicitly with its dependencies reads as  $F_i(q^2, s_1, s_2)$ . This form of the hadronic current is the most general one and constrained only by Lorentz invariance. For modes with an even number of kaons the normalization factor reads as  $N = \cos\theta_{\text{Cabibbo}}/F$ , otherwise  $N = \sin\theta_{\text{Cabibbo}}/F$ .

We leave the  $F_4$  contribution in the basis, even though it is of the order  $\sim m_\pi^2/q^2$  [17, 25, 15] for the three-pseudoscalar channels that we consider in this work. It plays a role in the low  $q^2$  region for the three-pion modes. We will neglect the corresponding contribution for the modes with kaons, i.e.,  $c_4 = 0$ . Among the three hadronic form factors which correspond to the axial-vector part of the hadronic tensor,  $(F_1, F_2, F_3)$ , only two are independent. We will keep the definition of  $F_1, F_2$  or  $F_3$ , exactly as shown in Eq. (3), which is the form used in TAUOLA since the beginning. However, linear combinations constructed from only two of these functions are in principle equally good. The decay channel dependent constants  $c_i$  are given in Table 1.

Decay mode ( $p_1, p_2, p_3$ )	$c_1$	$c_2$	$c_3$	$c_4$	$c_5$
$\pi^- \pi^- \pi^+$	1	- 1	0	1	0
$\pi^0 \pi^0 \pi^-$	1	- 1	0	1	0
$K^- \pi^- K^+$	1	- 1	0	0	1
$K^0 \pi^- K^0$	1	- 1	0	0	1
$K^- \pi^0 K^0$	0	1	- 1	0	- 1

Table 1: Coefficients for formula (3) in the isospin symmetry limit. Note, that in Ref. [11] different conventions were used and coefficients were affecting normalization too.

The theoretical assumptions behind the hadronic currents that we use are discussed in Section 7. In the model the results for all hadronic currents, with the exception of two-pion and two-kaon modes, are calculated in the isospin limit, therefore the corresponding hadronic form factors depend only on the average pion [ $m_\pi = (m_{\pi^0} + 2 \cdot m_{\pi^+})/3$ ] and kaon [ $m_K = (m_{K^0} + m_{K^+})/2$ ] masses, we relax the assumption later<sup>4</sup>. For the three-pseudoscalar modes every hadronic form factor consists of 3 parts: a chiral contribution (direct decay, without production of any intermediate resonance), one-resonance and double-resonance mediated processes. The results for the hadronic form factors are taken from Refs. [24, 25].

The channels we will present (together with the trivial decay – from the Monte Carlo point of view – into  $\pi\nu_\tau$  and  $K\nu_\tau$ ) represent more than 88 % of the hadronic width of  $\tau$  [31]. The dominant missing channels  $\tau \rightarrow \pi^+ \pi^- \pi^- \pi^0 \nu_\tau$  and  $\tau \rightarrow \pi^- \pi^0 \pi^0 \pi^0 \nu_\tau$ , which are together about 9.7 % of the hadronic width of  $\tau$ , are more difficult to control theoretically<sup>5</sup>.

<sup>4</sup>At first step we will take such assumption for our phase space generator as well. Later in the paper we will nonetheless return to proper masses, distinct for charged and neutral pseudoscalars. We will evaluate the numerical consequences, see Table 2.

<sup>5</sup> Several older options developed for these channels are provided for user convenience, but they will

Also attempts to describe  $\tau \rightarrow \pi^+\pi^-\pi^0\nu_\tau$  are relatively recent. They are technically compatible with our solution for TAUOLA currents and can be used simultaneously. It is documented in Ref. [33].

Let us now describe hadronic currents for each particular channel.

## 2.1 $\pi^-\pi^-\pi^+\nu_\tau$ and $\pi^0\pi^0\pi^-\nu_\tau$

Hadronic form factors for the three-pion modes have been calculated assuming the isospin symmetry<sup>6</sup>, as a consequence,  $m_{\pi^\pm} = m_{\pi^0}$ . The code for the current is given in `new-currents/RChL-currents/f3pi_rcht.f`.

The independent set of hadronic form factors  $F_i$ ,  $i = 1, \dots, 5$  is chosen as:  $F_1$ ,  $F_2$  and  $F_4$  ( $F_3 = 0$  then). The vector form factor vanishes for the three-pion modes due to the G-parity conservation [16, 43]:  $F_5 = 0$ . It is convenient to present the functions as

$$F_i = (F_i^X + F_i^R + F_i^{RR}) \cdot R^{3\pi}, \quad i = 1, 2, 4, \quad (4)$$

where  $F_i^X$  is the chiral contribution,  $F_i^R$  is the one resonance contribution and  $F_i^{RR}$  is the double-resonance part. The  $R^{3\pi}$  constant equals -1 for  $\pi^0\pi^0\pi^-$  and 1 for  $\pi^-\pi^-\pi^+$ .

For the convention defined by Eq. (3), the form factors  $F_i$  can be obtained from Ref. [24] with the replacements:

$$F_i(Q^2, s, t) \rightarrow F_i(q^2, s_1, s_2)/F, \quad i = 1, 2, 4, \quad (5)$$

where  $F$  was defined after Eq. (3). The form factors read:

$$\begin{aligned} F_1^X(q^2, s_1, s_2) &= -\frac{2\sqrt{2}}{3}, \\ F_1^R(q^2, s_1, s_2) &= \frac{\sqrt{2} F_V G_V}{3 F^2} \left[ \frac{3 s_1}{s_1 - M_\rho^2 - i M_\rho \Gamma_\rho(s_1)} - \right. \\ &\quad \left. \left( \frac{2G_V}{F_V} - 1 \right) \left( \frac{2q^2 - 2s_1 - s_3}{s_1 - M_\rho^2 - i M_\rho \Gamma_\rho(s_1)} + \frac{s_3 - s_1}{s_2 - M_\rho^2 - i M_\rho \Gamma_\rho(s_2)} \right) \right], \\ F_1^{RR}(q^2, s_1, s_2) &= \frac{4 F_A G_V}{3 F^2} \frac{q^2}{q^2 - M_A^2 - i M_A \Gamma_A(q^2)} \left[ - (\lambda' + \lambda'') \frac{3 s_1}{s_1 - M_\rho^2 - i M_\rho \Gamma_\rho(s_1)} \right. \\ &\quad \left. + H \left( \frac{s_1}{q^2}, \frac{m_\pi^2}{q^2} \right) \frac{2q^2 + s_1 - s_3}{s_1 - M_\rho^2 - i M_\rho \Gamma_\rho(s_1)} + H \left( \frac{s_2}{q^2}, \frac{m_\pi^2}{q^2} \right) \frac{s_3 - s_1}{s_2 - M_\rho^2 - i M_\rho \Gamma_\rho(s_2)} \right], \end{aligned} \quad (6)$$

not be documented here. Please see the README files stored in directory `new-currents/other-currents` for details.

<sup>6</sup>The inclusion of the complete first-order corrections to  $SU(2)$  symmetry is beyond our present scope. In particular, electromagnetic corrections arising at this order are neglected. We restrict ourselves, for the moment, to the ones given by the mass splittings between members of the same  $SU(2)$ -multiplet. These enter the kinematical factors and phase-space integrals. The model-independent electromagnetic corrections can be handled with PHOTOS [34, 35], while the structure-dependent corrections have been computed only for the one- and two-meson  $\tau$  decay modes (with only pions and kaons) in Refs. [36, 37, 38, 39]. Its implementation in generation with PHOTOS will follow work of Refs. [40, 41, 42].



where

$$H(x, y) = -\lambda_0 y + \lambda' x + \lambda'', \quad (7)$$

and

$$\begin{aligned} \lambda' &= \frac{F^2}{2\sqrt{2}F_A G_V}, \\ \lambda'' &= -\left(1 - 2\frac{G_V^2}{F^2}\right)\lambda', \\ 4\lambda_0 &= \lambda' + \lambda''. \end{aligned} \quad (8)$$

Bose symmetry implies that the form factors  $F_1$  and  $F_2$  are related  $F_2(q^2, s_2, s_1) = F_1(q^2, s_1, s_2)$  (the minus sign that comes from the definition of the hadronic current, Eq. (3), is included in  $c_2$ ).

The pseudoscalar form factor,  $F_4 = F_4^\chi + F_4^R$ , carries the contribution from both the direct vertex and the one-resonance mechanism of production:

$$\begin{aligned} F_4^\chi(q^2, s_1, s_2) &= \frac{2\sqrt{2}}{3} \frac{m_\pi^2 [3(s_3 - m_\pi^2) - q^2(1 + 2\kappa R^{3\pi})]}{2q^2(q^2 - m_\pi^2)}, \\ F_4^R(q^2, s_1, s_2) &= -\frac{\sqrt{2}F_V G_V}{3F^2} [\alpha_2(q^2, s_2, s_1) + \alpha_2(q^2, s_1, s_2)], \end{aligned} \quad (9)$$

where  $\kappa = 1$  for  $\tau^- \rightarrow \pi^- \pi^- \pi^+ \nu_\tau$ ,  $\kappa = 1/2$  for  $\tau^- \rightarrow \pi^0 \pi^0 \pi^- \nu_\tau$  and

$$\alpha_2(q^2, s_1, s_2) = \frac{3G_V}{F_V} \frac{s_1}{q^2} \frac{m_\pi^2}{q^2 - m_\pi^2} \frac{s_3 - s_2}{s_1 - M_\rho^2 - iM_\rho \Gamma_\rho(s_1)}. \quad (10)$$

The pseudoscalar form factor  $F_4$  is proportional to  $m_\pi^2/q^2$  [24], thus it is suppressed with respect to  $F_1$  and  $F_2$ . However, the pseudoscalar contribution can affect the  $q^2$  spectrum near the threshold<sup>7</sup>.

Besides the pion decay constant  $F$ , the results for the form factors  $F_i$  depend on some coupling constants of the model:  $F_V$  (we impose  $G_V = F^2/F_V$ ),  $F_A$  and the masses of the nonets of vector and axial-vector resonances ( $M_V$  and  $M_A$ ) in the chiral and large- $N_C$  limits. We follow Refs. [24, 25] and replace the masses used in the resonance Lagrangian with the masses of the corresponding physical states:  $M_V \rightarrow M_\rho$  and<sup>8</sup>  $M_A \rightarrow M_{a_1}$ .

To include the  $\rho'$  meson we follow Ref. [24], its Eq. (32). We insert Eq. (11) of the combined  $\rho$  and  $\rho'$  propagators into our Eqs. (6) and (10)

$$\frac{1}{M_\rho^2 - q^2 - iM_\rho \Gamma_\rho(q^2)} \longrightarrow \frac{1}{1 + \beta_{\rho'}} \left[ \frac{1}{M_\rho^2 - q^2 - iM_\rho \Gamma_\rho(q^2)} + \frac{\beta_{\rho'}}{M_{\rho'}^2 - q^2 - iM_{\rho'} \Gamma_{\rho'}(q^2)} \right]. \quad (11)$$

<sup>7</sup>Numerical results with and without  $F_4$  are presented in Section 4.2.

<sup>8</sup>In footnote <sup>56</sup> of Appendix C.2 we explain; the parameter  $M_A$  of the short-distance QCD constraints should not be identified with  $M_{a_1}$ . Our choice  $M_A \rightarrow M_{a_1}$  is not well founded, but can be easily changed at the time of fits to experimental data.

Impact<sup>9</sup> of the  $\rho'$  meson on the  $d\Gamma/dq^2$  spectrum can be seen from Fig. 3 of Ref. [24].

In the file `new-currents/RChL-currents/f3pi_rcht.f` the form factors  $F_1$ ,  $F_2$ ,  $F_4$  given by Eqs. (6)-(9) and with substitution (11) are coded. For completeness, let us remember that form factors  $F_3$  and  $F_5$  are equal to zero.

The only eventual isospin breaking will result from  $m_{\pi^\pm} \neq m_{\pi^0}$  used in the phase space generator embedded in `tauola.f`.

## 2.2 $K^- \pi^- K^+ \nu_\tau$ and $K^0 \pi^- \bar{K}^0 \nu_\tau$

Again isospin symmetry is assumed, therefore  $m_{\pi^\pm} = m_{\pi^0}$  and  $m_{K^0} = m_{K^\pm}$ . The code for the currents is given in `new-currents/RChL-currents/fkkpi.f`.

We will neglect the contribution from the pseudoscalar form factor  $F_4$  as it is proportional again to  $m_\pi^2/q^2$  [25]. We present the result for the non-zero form factors  $F_i$  in the same way as before:

$$F_i = F_i^X + F_i^R + F_i^{\text{RR}}, \quad i = 1, 2, 5. \quad (12)$$

Taking into account the convention for the current, Eq. (3), and the values of the  $c_i$  coefficients in Table 1 the result for the form factor can be obtained from Ref. [25] with the replacements:  $F_1(Q^2, s, t) \rightarrow F_2(q^2, s_2, s_1)/F$ ,  $F_2(Q^2, s, t) \rightarrow F_1(q^2, s_2, s_1)/F$ . Therefore, the form factor  $F_1$  reads

$$\begin{aligned} F_1^X(q^2, s_2, s_1) &= -\frac{\sqrt{2}}{3}, \\ F_1^R(q^2, s_2, s_1) &= -\frac{\sqrt{2}}{6} \frac{F_V G_V}{F^2} \left[ \frac{B^R(s_1, s_3, m_K^2, m_K^2)}{M_\rho^2 - s_2 - iM_\rho \Gamma_\rho(s_2)} + \frac{A^R(q^2, s_1, s_3, m_K^2, m_K^2, m_\pi^2)}{M_{K^*}^2 - s_1 - iM_{K^*} \Gamma_{K^*}(s_1)} \right], \\ F_1^{\text{RR}}(q^2, s_2, s_1) &= \frac{2}{3} \frac{F_A G_V}{F^2} \frac{q^2}{M_A^2 - q^2 - iM_A \Gamma_A(q^2)} \left[ \frac{B^{\text{RR}}(q^2, s_1, s_3, s_2, m_K^2, m_K^2, m_\pi^2)}{M_\rho^2 - s_2 - iM_\rho \Gamma_\rho(s_2)} \right. \\ &\quad \left. + \frac{A^{\text{RR}}(q^2, s_1, s_3, m_K^2, m_K^2, m_\pi^2)}{M_{K^*}^2 - s_1 - iM_{K^*} \Gamma_{K^*}(s_1)} \right]. \end{aligned} \quad (13)$$

where the functions  $A^R$ ,  $B^R$ ,  $A^{\text{RR}}$  and  $B^{\text{RR}}$  are defined in Appendix A and  $s_3$  is calculated from  $q^2$ ,  $s_1$ ,  $s_2$  and masses.

---

<sup>9</sup>A discussion on the implementation of the second (third) resonance nonet to the model can be found in Section 7.

The form factor  $F_2$  is given by

$$\begin{aligned}
F_2^X(q^2, s_2, s_1) &= F_1^X, \\
F_2^R(q^2, s_2, s_1) &= -\frac{\sqrt{2}}{6} \frac{F_V G_V}{F^2} \left[ \frac{A^R(q^2, s_2, s_3, m_K^2, m_\pi^2, m_K^2)}{M_\rho^2 - s_2 - iM_\rho \Gamma_\rho(s_2)} + \frac{B^R(s_2, s_3, m_K^2, m_\pi^2)}{M_{K^*}^2 - s_1 - iM_{K^*} \Gamma_{K^*}(s_1)} \right], \\
F_2^{RR}(q^2, s_2, s_1) &= \frac{2}{3} \frac{F_A G_V}{F^2} \frac{q^2}{M_A^2 - q^2 - iM_A \Gamma_A(q^2)} \left[ \frac{A^{RR}(q^2, s_2, s_3, m_K^2, m_\pi^2, m_K^2)}{M_\rho^2 - s_2 - iM_\rho \Gamma_\rho(s_2)} \right. \\
&\quad \left. + \frac{B^{RR}(q^2, s_2, s_3, s_1, m_K^2, m_\pi^2, m_K^2)}{M_{K^*}^2 - s_1 - iM_{K^*} \Gamma_{K^*}(s_1)} \right].
\end{aligned} \tag{14}$$

The vector form factor,  $F_5$ , arises from the chiral anomaly [44, 45] and the non-anomalous odd-intrinsic-parity amplitude [46]. It is obtained from Ref. [25] with the replacement  $F_3(Q^2, s, t) \rightarrow -F_5(q^2, s_2, s_1)/(4\pi^2 F^3)$ . It reads

$$\begin{aligned}
F_5^X(q^2, s_2, s_1) &= \sqrt{2}, \\
F_5^R(q^2, s_2, s_1) &= \frac{16\pi^2 G_V}{M_V} \left[ C^R(q^2, s_2, m_K^2, m_K^2, m_\pi^2) \left( \sin^2 \theta_V \frac{1 + \sqrt{2} \cot \theta_V}{M_\omega^2 - s_2 - iM_\omega \Gamma_\omega} \right. \right. \\
&\quad \left. \left. + \cos^2 \theta_V \frac{1 - \sqrt{2} \tan \theta_V}{M_\phi^2 - s_2 - iM_\phi \Gamma_\phi} \right) + \frac{C^R(q^2, s_1, m_K^2, m_\pi^2, m_K^2)}{M_{K^*}^2 - s_1 - iM_{K^*} \Gamma_{K^*}(s_1)} \right. \\
&\quad \left. - \frac{2 F_V}{G_V} \frac{D^R(q^2, s_2, s_1)}{M_\rho^2 - q^2 - iM_\rho \Gamma_\rho(q^2)} \right], \\
F_5^{RR}(q^2, s_2, s_1) &= -16\sqrt{2}\pi^2 F_V G_V \frac{1}{M_\rho^2 - q^2 - iM_\rho \Gamma_\rho(q^2)} \left[ \frac{C^{RR}(q^2, s_1, m_K^2)}{M_{K^*}^2 - s_1 - iM_{K^*} \Gamma_{K^*}(s_1)} + \right. \\
&\quad \left. C^{RR}(q^2, s_2, m_\pi^2) \left( \sin^2 \theta_V \frac{1 + \sqrt{2} \cot \theta_V}{M_\omega^2 - s_2 - iM_\omega \Gamma_\omega} + \cos^2 \theta_V \frac{1 - \sqrt{2} \tan \theta_V}{M_\phi^2 - s_2 - iM_\phi \Gamma_\phi} \right) \right],
\end{aligned} \tag{15}$$

where  $C^R$ ,  $D^R$  and  $C^{RR}$  are defined in Appendix A.

For the widths of the narrow resonances  $\omega$  and  $\phi$  the PDG [31] values are taken and the constant width approximation is followed. The parameter  $\theta_V$  defines the mass eigenstates  $\omega(782)$  and  $\phi(1020)$  [25] and is the mixing angle between the octet and singlet vector states  $\omega_8$  and  $\omega_0$ . In our numerical calculation we take the ideal mixing [ $\theta_V = \tan^{-1}(1/\sqrt{2})$ ]. In this limit, the contribution of the  $\phi(1020)$  meson in Eq. (15) vanishes<sup>10</sup>. This will be changed in future with fits to the data.

The file `new-currents/RChL-currents/fkkpi.f` contains the form factors  $F_1$ ,  $F_2$  and  $F_5$ . The form of Eqs. (13)-(15) is used. As one can see, the contribution from the excited states, e.g.  $\rho'$ ,  $\rho''$ , is not included in the  $KK\pi$  case, contrary to the three-pion one. The only eventual isospin breaking assumed will result from  $m_{\pi^\pm} \neq m_{\pi^0}$  and  $m_{K^\pm} \neq m_{K^0}$  used in the phase space generator embedded in `tauola.f`.

<sup>10</sup> On the other hand, one should keep in mind that the decay channel  $\tau^- \rightarrow \phi\pi^- \nu_\tau$  was observed by BaBar [47] and  $\tau^- \rightarrow \phi K^- \nu_\tau$  by Belle [48].

### 2.3 $K^- \pi^0 K^0 \nu_\tau$

The hadronic current of the  $K^- \pi^0 K^0 \nu_\tau$  decay mode is again obtained with isospin symmetry;  $m_{\pi^\pm} = m_{\pi^0}$  and  $m_{K^0} = m_{K^\pm}$ . The code for the currents is given in the file `new-currents/RChL-currents/fkk0pi0.f`.

If the momenta of the pseudoscalars are attributed as in Table 1, that is  $K^-(p_1)\pi^0(p_2)K^0(p_3)$ , then it is convenient to choose the independent set of hadronic form factors for the axial-vector part as  $F_2(q^2, s_2, s_3)$  and  $F_3(q^2, s_2, s_3)$ . We will neglect the contribution due to the pseudoscalar form factor  $F_4$  as it is again proportional to the square of pion mass over  $q^2$  [25]. Taking into account the constants  $c_i$  of Table 1 and Eq. (3), the result of Ref. [25] needs the replacements

$$\begin{aligned} F_2(Q^2, s, t) &\rightarrow F_3(q^2, s_2, s_3)/F, \quad F_1(Q^2, s, t) \rightarrow F_2(q^2, s_2, s_3)/F, \\ F_3(Q^2, s, t) &\rightarrow -F_5(q^2, s_2, s_3)/(4\pi^2 F^3). \end{aligned} \quad (16)$$

As before:

$$F_i = F_i^X + F_i^R + F_i^{RR}, \quad i = 2, 3, 5 \quad (17)$$

and

$$F_2^X(q^2, s_2, s_3) = -1, \quad (18)$$

$$\begin{aligned} F_2^R(q^2, s_2, s_3) &= -\frac{1}{6} \frac{F_V G_V}{F^2} \left[ \frac{B^R(s_2, s_1, m_K^2, m_\pi^2)}{M_{K^*}^2 - s_3 - iM_{K^*}\Gamma_{K^*}(s_3)} + 2 \frac{A^R(q^2, s_2, s_1, m_K^2, m_\pi^2, m_K^2)}{M_\rho^2 - s_2 - iM_\rho\Gamma_\rho(s_2)} \right. \\ &\quad \left. + \frac{A^R(q^2, s_1, s_2, m_\pi^2, m_K^2, m_K^2)}{M_{K^*}^2 - s_1 - iM_{K^*}\Gamma_{K^*}(s_1)} \right], \end{aligned}$$

$$\begin{aligned} F_2^{RR}(q^2, s_2, s_3) &= \frac{\sqrt{2} F_A G_V}{3} \frac{q^2}{F^2} \frac{1}{M_A^2 - q^2 - iM_A\Gamma_A(q^2)} \left[ \frac{B^{RR}(q^2, s_2, s_1, s_3, m_K^2, m_\pi^2, m_K^2)}{M_{K^*}^2 - s_3 - iM_{K^*}\Gamma_{K^*}(s_3)} \right. \\ &\quad \left. + 2 \frac{A^{RR}(q^2, s_2, s_1, m_K^2, m_\pi^2, m_K^2)}{M_\rho^2 - s_2 - iM_\rho\Gamma_\rho(s_2)} + \frac{A^{RR}(q^2, s_1, s_2, m_\pi^2, m_K^2, m_K^2)}{M_{K^*}^2 - s_1 - iM_{K^*}\Gamma_{K^*}(s_1)} \right], \end{aligned}$$

$s_3$  is calculated from  $q^2, s_1, s_2$  and masses. The contributions to  $F_3$  read

$$F_3^X(q^2, s_2, s_3) = 0, \quad (19)$$

$$\begin{aligned} F_3^R(q^2, s_2, s_3) &= -\frac{1}{6} \frac{F_V G_V}{F^2} \left[ \frac{A^R(q^2, s_3, s_1, m_K^2, m_K^2, m_\pi^2)}{M_{K^*}^2 - s_3 - iM_{K^*}\Gamma_{K^*}(s_3)} + 2 \frac{B^R(s_3, s_1, m_K^2, m_K^2)}{M_\rho^2 - s_2 - iM_\rho\Gamma_\rho(s_2)} \right. \\ &\quad \left. - \frac{A^R(q^2, s_1, s_3, m_K^2, m_K^2, m_\pi^2)}{M_{K^*}^2 - s_1 - iM_{K^*}\Gamma_{K^*}(s_1)} \right], \end{aligned}$$

$$F_3^{\text{RR}}(q^2, s_2, s_3) = \frac{\sqrt{2} F_A G_V}{3} \frac{q^2}{F^2 M_A^2 - q^2 - i M_A \Gamma_A(q^2)} \left[ \frac{A^{\text{RR}}(q^2, s_3, s_1, m_K^2, m_K^2, m_\pi^2)}{M_{K^*}^2 - s_3 - i M_{K^*} \Gamma_{K^*}(s_3)} \right. \\ \left. + 2 \frac{B^{\text{RR}}(q^2, s_3, s_1, s_2, m_K^2, m_K^2, m_\pi^2)}{M_\rho^2 - s_2 - i M_\rho \Gamma_\rho(s_2)} - \frac{A^{\text{RR}}(q^2, s_1, s_3, m_K^2, m_K^2, m_\pi^2)}{M_{K^*}^2 - s_1 - i M_{K^*} \Gamma_{K^*}(s_1)} \right].$$

The form factor  $F_5$  driven by the vector current is given by the sum of

$$F_5^{\text{X}}(q^2, s_2, s_3) = 0, \quad (20)$$

$$F_5^{\text{R}}(q^2, s_2, s_3) = \frac{8\sqrt{2}\pi^2 G_V}{M_V} \left[ \frac{C^{\text{R}}(q^2, s_3, m_K^2, m_\pi^2, m_K^2)}{M_{K^*}^2 - s_3 - i M_{K^*} \Gamma_{K^*}(s_3)} - \frac{C^{\text{R}}(q^2, s_1, m_K^2, m_\pi^2, m_K^2)}{M_{K^*}^2 - s_1 - i M_{K^*} \Gamma_{K^*}(s_1)} \right. \\ \left. - \frac{2F_V}{G_V} \frac{E^{\text{R}}(s_3, s_1)}{M_\rho^2 - q^2 - i M_\rho \Gamma_\rho(q^2)} \right],$$

$$F_5^{\text{RR}}(q^2, s_2, s_3) = -16\pi^2 F_V G_V \frac{1}{M_\rho^2 - q^2} \left[ \frac{C^{\text{RR}}(q^2, s_3, m_K^2)}{M_{K^*}^2 - s_3 - i M_{K^*} \Gamma_{K^*}(s_3)} \right. \\ \left. - \frac{C^{\text{RR}}(q^2, s_1, m_K^2)}{M_{K^*}^2 - s_1 - i M_{K^*} \Gamma_{K^*}(s_1)} \right],$$

where the new function  $E^{\text{R}}$ , as the previous ones, is defined in Appendix A.

The file `new-currents/RChL-currents/fkk0pi0.f` contains the form factors  $F_2$ ,  $F_3$  and  $F_5$ . Eqs. (18)-(20) are used. As one can see, the contributions from the excited states, e.g.  $\rho'$ ,  $K^{*'}$  are not included in the form factors of the  $\tau \rightarrow KK\pi\nu_\tau$  decay channels. This shall be an obvious future improvement resulting from the confrontation with the data.

The assumption that the eventual isospin breaking will result only from  $m_{\pi^\pm} \neq m_{\pi^0}$  and  $m_{K^\pm} \neq m_{K^0}$  as used in the phase space generator embedded in `tauola.f` is taken.

## 2.4 $\pi^- \pi^0 \nu_\tau$ , $\pi^0 K^- \nu_\tau$ , $\pi^- \bar{K}^0 \nu_\tau$ and $K^- K^0 \nu_\tau$

The two-pseudoscalar final states are simpler. They can be presented together in one subsection. The code for the hadronic currents of the  $\pi^- \pi^0 \nu_\tau$ ,  $K^- K^0 \nu_\tau$  and  $(K\pi)^- \nu_\tau$  modes is given, respectively, in files `new-currents/RChL-currents/frho_pi.f`, `new-currents/RChL-currents/fk0k.f` and `new-currents/RChL-currents/fkpi1.f`.

In the general case there are both vector and scalar form factors. In the isospin symmetry limit,  $m_{\pi^\pm} = m_{\pi^0}$ ,  $m_{K^\pm} = m_{K^0}$ , for both two-pion and two-kaon modes the scalar form factor vanishes and the corresponding channel is described by the vector form factor only<sup>11</sup>. Also for the  $K\pi$  mode we restrict ourselves at first to the vector form factor only, the scalar form factor will be properly included in Ref. [29].

<sup>11</sup>The scalar form factor appears only at next-to-leading order in SU(2) breaking and it can be safely neglected (see Ref. [36] for details).

For all three channels we use a parametrization for the vector form factor which is developed starting from the lowest-lying resonance contribution:

$$F_{PQ}^V(s) = F^{VMD}(s) \exp \left[ \sum_{P,Q} N_{loop}^{PQ} \frac{-s}{96\pi^2 F^2} ReA_{PQ}(s) \right], \quad (21)$$

where  $F^{VMD}$  is the contribution from the lightest vector resonance that can be exchanged in the process, and the exponentiation resums FSI effects (see Appendix E for a related discussion). The function  $A_{PQ}(s)$  is a loop function for two pseudoscalars with masses  $m_P$  and  $m_Q$ , and is presented in Appendix A.  $N_{loop}^{PQ}$  is a constant dictated by chiral symmetry for the different decay channels:

$$N_{loop}^{\pi^-\pi^0} = 1, \quad N_{loop}^{K^-K^0} = \frac{1}{2}, \quad N_{loop}^{K\pi} = N_{loop}^{K\eta} = \frac{3}{4}. \quad (22)$$

In the case of the two-pion mode, the theoretical calculation performed in the framework of R $\chi$ T [49] gives the following result for the form factor:

$$F_{\pi\pi}^V(s) = \frac{M_\rho^2}{M_\rho^2 - s - iM_\rho\Gamma_\rho(s)} \exp \left\{ \frac{-s}{96\pi^2 F^2} \left[ ReA_{\pi^-\pi^0}(s) + \frac{1}{2} ReA_{K^-K^0}(s) \right] \right\}, \quad (23)$$

if only  $\rho$  resonance is taken into account. The contribution of the excited resonances (both  $\rho'$  and  $\rho''$ ) modify the form factor of formula (23). Following Ref. [49] it takes the form

$$\begin{aligned} F_{\pi\pi}^V(s) = & \frac{M_\rho^2 + s(\gamma e^{i\phi_1} + \delta e^{i\phi_2})}{M_\rho^2 - s - iM_\rho\Gamma_\rho(s)} \exp \left\{ \frac{-s}{96\pi^2 F^2} \left[ ReA_{\pi^-\pi^0}(s) + \frac{1}{2} ReA_{K^-K^0}(s) \right] \right\} \\ & - \frac{s\gamma e^{i\phi_1}}{M_{\rho'}^2 - s - iM_{\rho'}\Gamma_{\rho'}(s)} \exp \left\{ \frac{-s\Gamma_{\rho'}}{\pi M_{\rho'}^3 \sigma_\pi^3(M_{\rho'}^2)} \left[ ReA_\pi(s) \right] \right\} \\ & - \frac{s\delta e^{i\phi_2}}{M_{\rho''}^2 - s - iM_{\rho''}\Gamma_{\rho''}(s)} \exp \left\{ \frac{-s\Gamma_{\rho''}}{\pi M_{\rho''}^3 \sigma_\pi^3(M_{\rho''}^2)} \left[ ReA_\pi(s) \right] \right\}, \end{aligned} \quad (24)$$

where the phase-space factor

$$\sigma_P(q^2) \equiv \sqrt{1 - 4m_P^2/q^2} \quad (25)$$

is used. The function  $A_P$  is the same loop function  $A_{PQ}$  defined in (45), but in the limit of equal masses. It is given in Appendix A. In our file `new-currents/RChL-currents/frho_pi.f` the form factor of formula (24) is used.

The two-kaon vector form factor is written following Ref. [26] as

$$F_{KK}^V(s) = \frac{M_\rho^2}{M_\rho^2 - s - iM_\rho\Gamma_\rho(s)} \exp \left\{ \frac{-s}{96\pi^2 F^2} \left[ ReA_{\pi^-\pi^0}(s) + \frac{1}{2} ReA_{K^-K^0}(s) \right] \right\}. \quad (26)$$

One can see the expression for the kaon vector form factors coincides with the pion form factor from Eq. (23).

The excited resonances have not been taken into account in Eq. (26) following Ref. [26]. However, their implementation along the lines of Eq. (24) is simple. The file `new-currents/RChL-currents/fk0k.f` contains both<sup>12</sup> forms of the two-kaon form factor (24) and (26).

For the  $K\pi$  mode we applied the result of Ref. [27] Eq.(5), which reads<sup>13</sup>:

$$F_{K\pi}^V(s) = \left( \frac{M_{K^*}^2 + s\gamma_{K\pi}}{M_{K^*}^2 - s - iM_{K^*}\Gamma_{K^*}(s)} - \frac{s\gamma_{K\pi}}{M_{K^{*\prime}}^2 - s - iM_{K^{*\prime}}\Gamma_{K^{*\prime}}(s)} \right) \exp \left\{ \frac{-s}{128\pi^2 F^2} \left[ \text{Re}A_{K\pi}(s) + \text{Re}A_{K\eta}(s) \right] \right\}. \quad (27)$$

Note that due to the FSI effects, the form factor  $F_{K\pi}^V(0) \neq 1$ .

The  $m_{\pi^\pm} \neq m_{\pi^0}$  and  $m_{K^\pm} \neq m_{K^0}$  used in the phase space Monte Carlo generator, and discussed numerically later in the paper, will be the only isospin breaking assumed. However, we plan to include electromagnetic corrections to  $\tau \rightarrow \pi^- \pi^0 \nu_\tau$  decays in the future (see <sup>6</sup>).

### 3 Energy-dependent widths of resonances

In this section we collect the formulas to calculate the energy-dependent width of the resonances  $\rho$ ,  $\rho'$ ,  $\rho''$ ,  $K^*$ ,  $K^{*\prime}$  and  $a_1$ . They were used in the previous section as ingredients for the construction of hadronic currents. From the technical side their calculation requires integration of the appropriate matrix elements over the phase space. In this way, for example, unitarity constraints are taken into account [24, 51, 52].

The energy-dependent width of  $\rho(770)$  resonance, calculated in the  $SU(2)$  limit ( $m_{\pi^\pm} = m_{\pi^0}$ ,  $m_{K^\pm} = m_{K^0}$ ), is given [52] as

$$\Gamma_\rho(q^2) = \frac{M_\rho q^2}{96\pi F^2} \left[ \sigma_\pi^3(q^2)\theta(q^2 - 4m_\pi^2) + \frac{1}{2}\sigma_K^3(q^2)\theta(q^2 - 4m_K^2) \right]. \quad (28)$$

The phase-space factor  $\sigma_\pi$  is defined in Eq. (25), the  $2\pi$  and  $2K$  loops are included. This form of the  $\rho$  width is used in modes of three pseudoscalars.

<sup>12</sup>By default, our program runs with the  $K^0 K^-$  vector form factor of Eq. (26). However, changing the value of the parameter `FFKKVEC = 0` to `FFKKVEC = 1` in `value.parameter.f` allows to run the code with the form factor of Eq. (24). Numerical effects due to the inclusion of the excited resonances are given in Section 5.4.

<sup>13</sup>By default, our program runs with the  $K\pi$  vector form factor of Eq. (27). However, changing the value of the parameter `FFKPIVEC = 1` to `FFKPIVEC = 0` the code will run with the form factor given in Eqs. (17), (18) of Ref. [50]. For discussion, see Section 5.4.

In the two-pion and two-kaon modes  $SU(2)$  breaking effects were taken into account in the  $\rho$  off-shell width

$$\Gamma_\rho(q^2) = \frac{M_\rho q^2}{96\pi F^2} \left[ \theta(q^2 - thr_{\pi\pi}) \lambda^{3/2} \left( 1, \frac{m_{\pi^+}^2}{q^2}, \frac{m_{\pi^0}^2}{q^2} \right) + \frac{1}{2} \theta(q^2 - thr_{KK}) \lambda^{3/2} \left( 1, \frac{m_{K^+}^2}{q^2}, \frac{m_{K^0}^2}{q^2} \right) \right], \quad (29)$$

where  $\lambda(x, y, z) = (x - y - z)^2 - 4yz$ ,  $thr_{\pi\pi} = (m_{\pi^+} + m_{\pi^0})^2$  and  $thr_{KK} = (m_{K^+} + m_{K^0})^2$ .

At this stage the widths of the  $\rho'(1465)$  and  $\rho''(1700)$  mesons are modeled as decays to two pions,

$$\Gamma_{\rho'}(q^2) = \Gamma_{\rho'} \frac{q^2}{M_{\rho'}^2} \frac{\sigma_\pi^3(q^2)}{\sigma_\pi^3(M_{\rho'}^2)} \theta(q^2 - 4m_\pi^2), \quad (30)$$

with  $\Gamma_{\rho'} \equiv \Gamma_{\rho'}(M_{\rho'}^2)$ .

The energy-dependent width of the  $K^*(892)$  resonance is given, in the  $SU(2)$  limit ( $m_{\pi^\pm} = m_{\pi^0}$ ,  $m_{K^\pm} = m_{K^0}$ ), in Ref. [53]. It is related to  $\Gamma_\rho(q^2)$  by chiral symmetry. It reads:

$$\Gamma_{K^*}(q^2) = \frac{M_{K^*} q^2}{128\pi F^2} \left[ \lambda^{3/2} \left( 1, \frac{m_K^2}{q^2}, \frac{m_\pi^2}{q^2} \right) \theta(q^2 - thr_{K\pi}) + \lambda^{3/2} \left( 1, \frac{m_K^2}{q^2}, \frac{m_\eta^2}{q^2} \right) \theta(q^2 - thr_{K\eta}) \right], \quad (31)$$

with  $thr_{K\pi} = (m_K + m_\pi)^2$  and  $thr_{K\eta} = (m_K + m_\eta)^2$ .

Formula (31) is used for the  $KK\pi$  modes whereas for the  $K\pi$  modes we use the following result (Eq. (4) from Ref. [27])

$$\Gamma_{K^*}(q^2) = \Gamma_{K^*} \frac{q^2}{M_{K^*}^2} \frac{\lambda^{3/2} \left( 1, \frac{m_K^2}{q^2}, \frac{m_\pi^2}{q^2} \right) \theta(q^2 - thr_{K\pi}) + \lambda^{3/2} \left( 1, \frac{m_K^2}{q^2}, \frac{m_\eta^2}{q^2} \right) \theta(q^2 - thr_{K\eta})}{\lambda^{3/2} \left( 1, \frac{m_K^2}{M_{K^*}^2}, \frac{m_\pi^2}{M_{K^*}^2} \right) + \lambda^{3/2} \left( 1, \frac{m_K^2}{M_{K^*}^2}, \frac{m_\eta^2}{M_{K^*}^2} \right)}. \quad (32)$$

From Eq. (4) of Ref. [27] we have

$$\Gamma_{K^*} \equiv \Gamma_{K^*}(M_{K^*}^2) = \frac{G_V^2 M_{K^*}^3}{64\pi F^4} \left[ \lambda^{3/2} \left( 1, \frac{m_K^2}{M_{K^*}^2}, \frac{m_\pi^2}{M_{K^*}^2} \right) + \lambda^{3/2} \left( 1, \frac{m_K^2}{M_{K^*}^2}, \frac{m_\eta^2}{M_{K^*}^2} \right) \right], \quad (33)$$

however, we prefer to write down Eq. (32) in terms of the width ( $\Gamma_{K^*}$ ), see discussion after Eq. (17) in Ref. [27]. The width of  $K^*(1410)$  is modelled as a decay to  $K\pi$  and reads

$$\Gamma_{K^{*'}}(q^2) = \Gamma_{K^{*'}} \frac{q^2}{M_{K^{*'}}^2} \frac{\lambda^{3/2} \left( 1, \frac{m_K^2}{q^2}, \frac{m_\pi^2}{q^2} \right)}{\lambda^{3/2} \left( 1, \frac{m_K^2}{M_{K^{*'}}^2}, \frac{m_\pi^2}{M_{K^{*'}}^2} \right)} \theta(q^2 - thr_{K\pi}). \quad (34)$$

For the energy dependence of the  $a_1$  resonance width<sup>14</sup> we use<sup>15</sup> [24]

$$\begin{aligned} \Gamma_{a_1}(q^2) &= 2\Gamma_{a_1}^\pi(q^2) \theta(q^2 - 9m_\pi^2) \\ &+ 2\Gamma_{a_1}^{K^\pm}(q^2) \theta(q^2 - (m_\pi + 2m_K)^2) + \Gamma_{a_1}^{K^0}(q^2) \theta(q^2 - (m_\pi + 2m_K)^2), \end{aligned} \quad (35)$$

<sup>14</sup>Calculation of  $a_1$  width from  $F_i$  was already used in Refs. [5, 12, 54].

<sup>15</sup>There is an additional factor  $1/F^2$  here and in Eq. (38) compared with the definition, e.g. in Refs. [24, 25]. This is related to the normalization of our form factors  $F_1$ ,  $F_2$  and  $F_3$ . See explanation prior to the Eqs. (6), (13) and (18).



where

$$\Gamma_{a_1}^{\pi,K}(q^2) = \frac{-S}{192(2\pi)^3 F_A^2 F^2 M_{a_1}} \left( \frac{M_{a_1}^2}{q^2} - 1 \right)^2 \int dsdt (V_1^\mu F_1 + V_2^\mu F_2 + V_3^\mu F_3)^{\pi,K} \left( (V_{1\mu} F_1 + V_{2\mu} F_2 + V_{3\mu} F_3)^{\pi,K} \right)^* \quad (36)$$

stands for the contribution from the individual three-pion and (two kaons - one pion) absorptive cuts. Here

$$V_i^\mu = c_i T^{\mu\nu} (p_j - p_k)_\nu, \quad i \neq j \neq k = 1, 2, 3, \quad (37)$$

with the coefficients  $c_i$  appearing in Table 1.

In summary,  $\Gamma_{a_1}^\pi(q^2)$  is the contribution of the  $\pi^- \pi^- \pi^0$  and  $\pi^0 \pi^0 \pi^-$  cuts,  $\Gamma_{a_1}^{K^\pm}(q^2)$  of the  $K^- \pi^- K^+$  and  $K^0 \pi^- \bar{K}^0$  cuts, and finally the  $K^- \pi^0 K^0$  contribution gives rise to the term  $\Gamma_{a_1}^{K^0}(q^2)$ . The form factors  $F_i$  are presented in Sections 2.1, 2.2 and 2.3. The symmetry factor is defined as  $S = 1/n!$ , where  $n$  denotes the number of identical particles in the final state.

For reference, we include the formula for the spectral function, the  $q^2$ -spectrum for the processes  $\tau \rightarrow 3$  pseudoscalars  $\nu_\tau$  of this work<sup>16</sup>

$$\frac{d\Gamma}{dq^2} = \frac{G_F^2 |V_{ud}|^2}{128(2\pi)^5 M_\tau F^2} \left( \frac{M_\tau^2}{q^2} - 1 \right)^2 \int dsdt \left[ W_{SA} + \frac{1}{3} \left( 1 + 2 \frac{q^2}{M_\tau^2} \right) (W_A + W_B) \right], \quad (38)$$

where

$$\begin{aligned} W_A &= -(V_1^\mu F_1 + V_2^\mu F_2 + V_3^\mu F_3)(V_{1\mu} F_1 + V_{2\mu} F_2 + V_{3\mu} F_3)^*, \quad (39) \\ W_B &= \frac{1}{64\pi^4 F^4} [stu + (m_{K,\pi}^2 - m_\pi^2)(q^2 - m_{K,\pi}^2)s + m_{K,\pi}^2(2m_\pi^2 - q^2)q^2 - m_{K,\pi}^2 m_\pi^4] |F_5|^2, \\ W_{SA} &= q^2 |F_4|^2. \end{aligned}$$

The following phase space integration limits have to be used

$$\int dsdt = \int_{4m_{K,\pi}^2}^{(\sqrt{q^2 - m_\pi})^2} ds \int_{t_-(s)}^{t_+(s)} dt, \quad (40)$$

where

$$t_\pm(s) = \frac{1}{4s} \left\{ (q^2 - m_\pi^2)^2 - [\lambda^{1/2}(q^2, s, m_\pi^2) \mp \lambda^{1/2}(m_{K,\pi}^2, m_{K,\pi}^2, s)]^2 \right\}. \quad (41)$$

The necessary functions are located in files `new-currents/RChL-currents/funct_rpt.f` and `new-currents/RChL-currents/wid_a1_fit.f`.

---

<sup>16</sup>Our testing programs feature a calculation of spectral functions, including those of the formula (39). However, we will not elaborate on this point here, even though it is important for future data analysis [9], where results of Ref. [13] are proposed to be used. We expect that a Monte Carlo sample will be used instead of semianalytical Eq. (38).

## 4 Benchmark calculations for three-pion mode

Since Ref. [11] has been published, numerical tests of TAUOLA Monte Carlo functioning have not been repeated in a systematic way, despite the technical precision requirements are much higher now and reach sub-per mil level. Prior to physics oriented comparisons between analytical (numerical integration) and Monte Carlo calculations, we need to revisit numerical stability of the generator and of multiple numerical integration, used in semianalytical calculations accompanying generation and its tests as well.

We will use the decay channel  $\tau \rightarrow \pi^- \pi^- \pi^+ \nu_\tau$  to demonstrate our tests of Monte Carlo. For other channels, technical tests will be skipped from documentation<sup>17</sup> even though new issues absent in the  $\tau \rightarrow \pi^- \pi^- \pi^+ \nu_\tau$  case can appear. A good example is numerical stability at phase space edges of presamplers for relatively narrow resonances such as  $K^*$  in  $\tau \rightarrow K \pi \nu_\tau$  decay. In this case, for long runs square root of a negative number may have appeared because of rounding errors; an appropriate correction to the code was introduced. Such long runs were never performed in the past for this channel. Our tests were indeed long. In some cases, for variables counting crude events we have even run over the allowed maximum ( $\sim 2 \cdot 10^9$ ) for FORTRAN INTEGER type.

To avoid problems with multidimensional integration of the  $a_1$ -meson propagator which is rapidly-changing as a function of its arguments, we first tabulated the  $\Gamma_{a_1}(q^2)$  of Eq. (35). The code for tabulation is located in `new-currents/RChL-currents/tablet`<sup>18</sup>. Then we use linear interpolation to get the value of the  $a_1$  width at required  $q^2$ . To integrate over  $s$  and  $t$  variables the Gauss integration method has been used. The produced distribution has been checked to be numerically stable<sup>19</sup>.

### 4.1 Technical test

Before we can go to the presentation of simulation results, where physical currents are used, let us start with the simplified cases. We will begin with the calculation for  $\tau \rightarrow \pi^- \pi^- \pi^+ \nu_\tau$  where  $F_1 = F = 0.0924$  GeV, other form factors are set to zero ( $F_2 = 0$ ,  $F_4 = 0$ ) and  $m_{\pi^\pm} = m_{\pi^0} = 0.13804$  GeV. It is an important starting point, it helps to adjust conventions of normalization constants in TAUOLA Monte Carlo and analytical calculations. Phase space integration is free from singularities resulting from the matrix elements. Nonetheless, corresponding presamplers can be verified. Numerical integration is rather quick as there is no need of invoking time consuming functions. That is why it is important to perform this check with a precision higher than for later tests.

---

<sup>17</sup>Directory `new-currents/RChL-currents/cross-check` is devoted to such tests. The README file explains technical details.

<sup>18</sup>Technical details of the calculations, which are quite independent from parts of the code loaded with TAUOLA, are explained in README files of this directory and its subdirectories.

<sup>19</sup>The source code of the integration routine `gauss` has been taken from CERN program library [55]. Tests are provided in `new-currents/RChL-currents/cross-checks`. Cross-check by linear interpolation of the  $q^2$  distribution from the neighbouring points demonstrates that the fluctuations due to numerical problems of integration are absent, the results are continuous, whereas the result produced with the integration method VEGAS [56] had a tendency to fluctuate.

The total rate we obtained from a Monte Carlo run of  $6 \cdot 10^6$  events was  $(2.7414 \pm 0.01\%) \cdot 10^{-17}$  GeV. For semianalytical numerical integration we obtain  $(2.7410 \pm 0.02\%) \cdot 10^{-17}$  GeV (with  $2 \cdot 10^{-4}$  precision tag). A difference of 0.015% was found. This technical test performs better than could be achieved at time of work for reference [11]. Statistical samples are larger by 3 orders of magnitude than what could have been used at that time.

For completeness, let us provide a plot of  $\frac{d\Gamma}{dq^2}$  generated from Monte Carlo divided by the semianalytical (numerical integration was used) result for this spectrum. Reasonable agreement is found, see Fig. 1.

Triple Gaussian integration is used for the analytical calculation and double Gaussian integration enters as well into the current calculation to be used in matrix elements of Monte Carlo generation. That is why pretabulation for the  $a_1$  width,  $\Gamma_{a_1}(q^2)$ , is convenient as it speeds generation enormously. This represents another technical feature being tested by normalization study and figures like Fig. 1.

Technical tests, as the one we discuss now, belong to the group of comparison booklets collected in the Web page [28].

## 4.2 Test with semirealistic parameters

Let us now introduce the physical content of the current, keeping at first  $m_{\pi^\pm} = m_{\pi^0} = 0.13804$  GeV and dropping out statistical factor  $\frac{1}{2}$  of two identical  $\pi$ 's. Agreement between Monte Carlo and semianalytical calculation should be  $\sim 0.01\%$  again.

We take  $F_1$  as given by Eq. (6), but all other currents are set to 0. Our numerical results for the rate from numerical integration,  $(1.8721 \pm 0.02\%) \cdot 10^{-13}$  GeV, and from Monte Carlo generation,  $(1.8722 \pm 0.01\%) \cdot 10^{-13}$  GeV (run with  $6 \cdot 10^6$  events), agree well. The difference is only 0.005% thus compatible with statistical error of generated sample. Comparison of differential distributions, analogue to Fig. 1, is available from the Web page [28]. For the next step we choose the  $F_1$  and  $F_2$  form factors according to Eq. (6),  $F_4 = 0$ . Numerical results are:  $(4.2015 \pm 0.02\%) \cdot 10^{-13}$  GeV for semianalytical calculation and  $(4.2023 \pm 0.01\%) \cdot 10^{-13}$  GeV for Monte Carlo generation. The difference is 0.03%, as expected. The figures are again available from Ref. [28].

Finally, we consider the result for the total width predicted by Resonance Chiral Theory, given by the  $F_1$ ,  $F_2$  and  $F_4$  contributions in Eqs. (6) and (9). The  $F_4$  form factor does not affect the value of the width at our precision and in this case it is  $(4.2025 \pm 0.01\%) \cdot 10^{-13}$  GeV (run with  $6 \cdot 10^6$  events).

The above comparisons check also that the differential distribution  $d\Gamma/dq^2$  in  $\tau \rightarrow 3\pi\nu_\tau$  is numerically stable. In particular that it is not affected by numerical problems due to double Gaussian integration. We have also checked, that if the function value has been obtained from interpolation of neighboring  $q^2$ 's, the difference with the value calculated directly was appropriately small as should be expected<sup>20</sup>.

---

<sup>20</sup> The appropriate program for a test is available in the directory `new-currents/RChL-currents/cross-check/check_analyticity/check_analyt_3pi`.

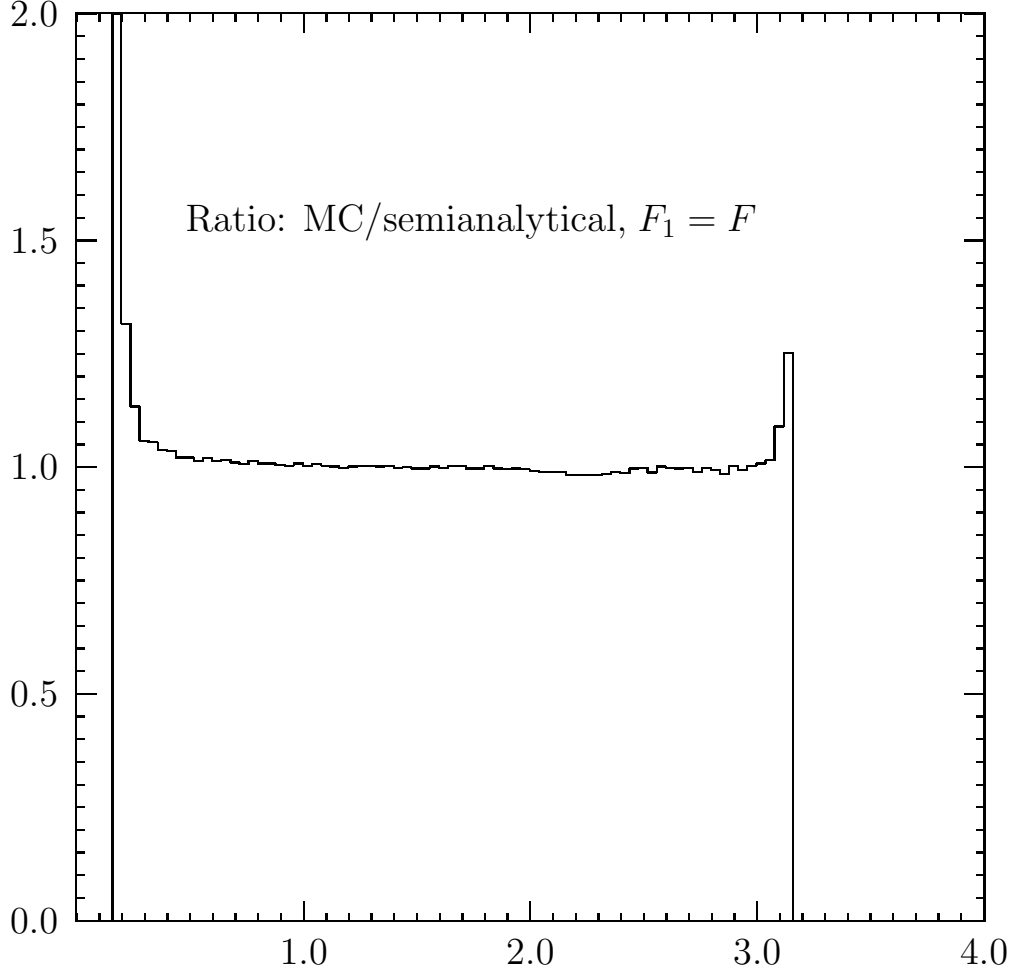


Figure 1: An example of a figure included in tests collected in project web page [28]. The ratio of the histogram and analytical formula is shown for the  $\frac{d\Gamma}{dq^2}$  in  $\tau \rightarrow \pi^- \pi^- \pi^+ \nu_\tau$  decay mode. Only  $F_1 = F$  is non-zero. Normalization is not adjusted. A statistical sample of  $6 \cdot 10^6$  events was used and semirealistic initialization as explained in this section. Agreement within statistical errors is found. Fluctuations at the ends of the spectra are due to substantially less populated bins of that region. These tests represent a technical test not only of Monte Carlo generation but also for semianalytical numerical integration.

Channel	Width, [GeV]		
	PDG	Equal masses	Phase space with masses
$\pi^- \pi^0$	$(5.778 \pm 0.35\%) \cdot 10^{-13}$	$(5.2283 \pm 0.005\%) \cdot 10^{-13}$	$(5.2441 \pm 0.005\%) \cdot 10^{-13}$
$\pi^0 K^-$	$(9.72 \pm 3.5\%) \cdot 10^{-15}$	$(8.3981 \pm 0.005\%) \cdot 10^{-15}$	$(8.5810 \pm 0.005\%) \cdot 10^{-15}$
$\pi^- \bar{K}^0$	$(1.9 \pm 5\%) \cdot 10^{-14}$	$(1.6798 \pm 0.006\%) \cdot 10^{-14}$	$(1.6512 \pm 0.006\%) \cdot 10^{-14}$
$K^- K^0$	$(3.60 \pm 10\%) \cdot 10^{-15}$	$(2.0864 \pm 0.007\%) \cdot 10^{-15}$	$(2.0864 \pm 0.007\%) \cdot 10^{-15}$
$\pi^- \pi^- \pi^+$	$(2.11 \pm 0.8\%) \cdot 10^{-13}$	$(2.1013 \pm 0.016\%) \cdot 10^{-13}$	$(2.0800 \pm 0.017\%) \cdot 10^{-13}$
$\pi^0 \pi^0 \pi^-$	$(2.10 \pm 1.2\%) \cdot 10^{-13}$	$(2.1013 \pm 0.016\%) \cdot 10^{-13}$	$(2.1256 \pm 0.017\%) \cdot 10^{-13}$
$K^- \pi^- K^+$	$(3.17 \pm 4\%) \cdot 10^{-15}$	$(3.7379 \pm 0.024\%) \cdot 10^{-15}$	$(3.8460 \pm 0.024\%) \cdot 10^{-15}$
$K^0 \pi^- \bar{K}^0$	$(3.9 \pm 24\%) \cdot 10^{-15}$	$(3.7385 \pm 0.024\%) \cdot 10^{-15}$	$(3.5917 \pm 0.024\%) \cdot 10^{-15}$
$K^- \pi^0 K^0$	$(3.60 \pm 12.6\%) \cdot 10^{-15}$	$(2.7367 \pm 0.025\%) \cdot 10^{-15}$	$(2.7711 \pm 0.024\%) \cdot 10^{-15}$

Table 2: The  $\tau$  decay partial widths. For each channel, the PDG value [31] is compared with numerical results of Monte Carlo integration of our currents. The third column includes results with isospin averaged masses, whereas for the last column physical masses were used. Comparison of the last two columns enumerates the numerical effect of physical masses, breaking the assumption of isospin symmetry in a potentially uncontrolled way. Further results for individual decay channels are given in Subsections of Section 5.

## 5 Numerical results for two and three-pseudoscalar channels

In the previous section we have presented examples of technical tests. Let us now concentrate on numerical results, corresponding to the most refined options of the currents included in our distribution tar-ball<sup>21</sup> which are of physics interest.

In the phase space generation, we will take into account the differences between neutral and charged pion and kaon masses, physical values will be taken. This has to be done to obtain proper kinematic configurations. On the other hand, this choice breaks constraints resulting from isospin symmetry (see <sup>6</sup>) in a potentially uncontrolled way. That is why we collect numerical results from Monte Carlo calculation in the form of Table 2, where the partial widths from Particle Data Group compilation [31] are compared with our results obtained with isospin-averaged pseudoscalar masses and with the physical ones.

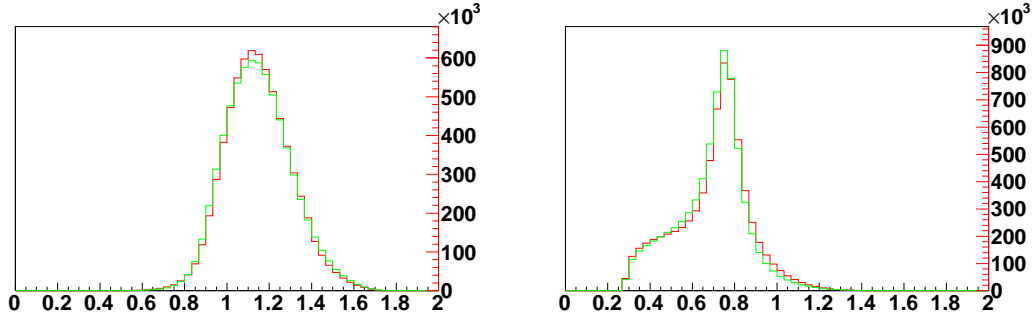


Figure 2: The  $\tau \rightarrow \pi^- \pi^- \pi^+ \nu_\tau$  decay: comparison of distributions for TAUOLA cleo current [14] and for our new current. On the left-hand side, the plot of  $\pi^- \pi^- \pi^+$  invariant mass is shown and on the right-hand side  $\pi^+ \pi^-$  invariant mass is given. Green histograms (light grey) are for the new current, red (darker grey) are for TAUOLA cleo. Distributions for the  $\tau \rightarrow \pi^0 \pi^0 \pi^- \nu_\tau$  decay coincide with the ones for  $\tau \rightarrow \pi^- \pi^- \pi^+ \nu_\tau$ .

### 5.1 $\pi^- \pi^- \pi^+ \nu_\tau$ and $\pi^0 \pi^0 \pi^- \nu_\tau$

Let us now turn to numerical results for the  $\tau \rightarrow 3\pi \nu_\tau$  decays obtained with our currents of Subsection 2.1. From the semianalytical calculation of partial width we get  $(2.10073 \pm 0.02\%) \cdot 10^{-13}$  GeV for  $\tau \rightarrow \pi^- \pi^- \pi^+ \nu_\tau$  decay, and  $(2.10072 \pm 0.02\%) \cdot 10^{-13}$  GeV for  $\tau \rightarrow \pi^0 \pi^0 \pi^- \nu_\tau$ , practically the same value. The approximation of the equal masses for  $\pi^\pm$  and  $\pi^0$  has been taken. In this case the Monte Carlo results are identical for  $\pi^- \pi^- \pi^+$  and  $\pi^0 \pi^0 \pi^-$  final states<sup>22</sup>; we have obtained  $(2.1013 \pm 0.016\%) \cdot 10^{-13}$  GeV.

For the physical, i.e., distinct  $m_{\pi^\pm}$  and  $m_{\pi^0}$ , masses we have obtained  $(2.0800 \pm 0.017\%) \cdot 10^{-13}$  GeV for  $\pi^- \pi^- \pi^+$  and  $(2.1256 \pm 0.017\%) \cdot 10^{-13}$  GeV for  $\pi^0 \pi^0 \pi^-$  mode. The difference for the distributions is too small to be seen and we present plots for the  $\pi^0 \pi^0 \pi^-$  case. Only two example plots are given in Fig. 2. We point the reader to the web page [28], for the booklet of comparisons obtained with MC-TESTER [57]. The figures for  $d\Gamma/dq^2$  spectrum from Monte Carlo and analytical calculations are also available from the plots of the Web page [28].

From the technical point of view to separate generation of the two  $3\pi$  sub-channels one has to set the `BRA1 = 0` for the  $\pi^0 \pi^0 \pi^-$  mode, and `BRA1 = 1` for the  $\pi^- \pi^- \pi^+$ , (e.g., in routine `INITDK`, which is defined in our demonstration program `new-currents/Installation/demo-standalone/taumain.f`).

An attempt on comparisons of the new model distributions and experimental data is also given later in the paper, in Section 5.5.

<sup>21</sup>For the convenience of updates, we have prepared Appendix D, to be modified in the versions of the present paper to be included in the tar-ball. It summarizes elementary installation benchmark results, that is the branching ratios calculated by the Monte Carlo.

<sup>22</sup>The chiral contribution  $F_4^X(q^2, s_1, s_2)$ , Eq. (9), differs for  $\pi^- \pi^- \pi^+$  and  $\pi^0 \pi^0 \pi^-$ . However,  $F_4(q^2, s_2, s_1)$  does not affect sizably the width.

## 5.2 $K^-\pi^-K^+\nu_\tau$ and $K^0\pi^-\bar{K}^0\nu_\tau$

As in the case of  $3\pi$  decay modes, the Monte Carlo generated distributions are relegated to the project web page [28]. In particular successful checks with the analytic function for  $d\Gamma/dq^2$  taken from Ref. [25] are shown there. In the following, we present figures 3 and 4 comparing the two histograms obtained with our new and cleo versions of TAUOLA currents. The differences are substantial. CLEO Collaboration [58, 21] introduced an

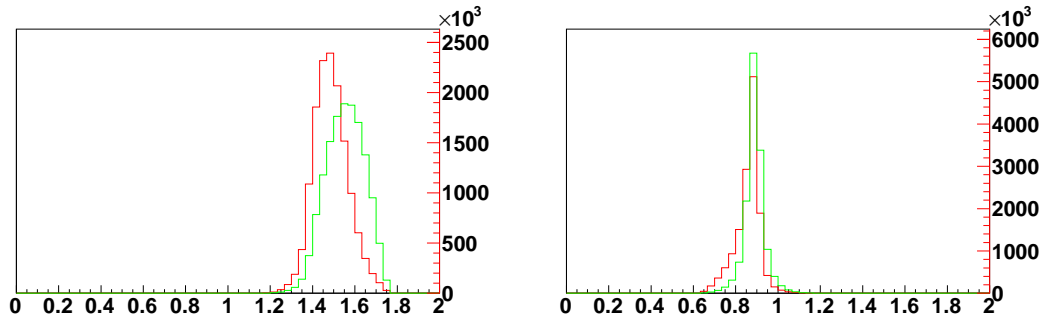


Figure 3: The  $\tau \rightarrow K^-\pi^-K^+\nu_\tau$  decay: comparison of distributions for TAUOLA cleo current [14] and for our new current. On the left-hand side, plot of  $K^-\pi^-K^+$  invariant mass is shown and on the right-hand side  $K^+\pi^-$  invariant mass is given. Green histograms (light grey) are for the new current, red (darker grey) are for TAUOLA cleo.

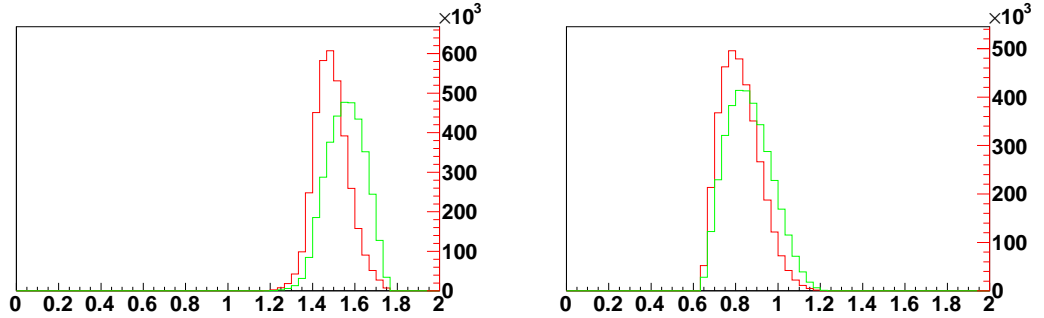


Figure 4: The  $\tau \rightarrow K^0\pi^-\bar{K}^0\nu_\tau$  decay: comparison of distributions for TAUOLA cleo current [14] and for our new current. On the left-hand side, plot of  $K_S^0K_S^0\pi^-$  invariant mass is shown and on the right-hand side  $K_S^0\pi^-$  invariant mass is given. Green histograms (light grey) are for the new current, red (darker grey) are for TAUOLA cleo.

ad-hoc parameter violating a property stemming directly from QCD, the normalization of the vector form factor given by the chiral anomaly [59]. Of course, in our new current we are not taking into account excited resonances. In the past, two couplings could only be estimated because of unavailability of data to determine them from a fit. These aspects

can (and should) be improved at the time of confronting with the data<sup>23</sup>.

Let us now turn to the decay widths. The result for  $SU(2)$  symmetric masses from TAUOLA with a sample of  $2 \cdot 10^6$  events is  $\Gamma = (3.7379 \pm 0.024\%) \cdot 10^{-15}$  GeV for  $K^- \pi^- K^+$  and  $\Gamma = (3.7385 \pm 0.024\%) \cdot 10^{-15}$  GeV for  $K^0 \pi^- \bar{K}^0$ . The difference for the partial width of the two channels is within statistical error. The analytical result is the same for both channels and was found to be  $(3.7383 \pm 0.02\%) \cdot 10^{-15}$  GeV. It agrees with the ones of Monte Carlo.

For physical masses of the pseudoscalars, the Monte Carlo results for  $K^- \pi^- K^+$  and  $K^0 \pi^- \bar{K}^0$  are, respectively,  $\Gamma = (3.8460 \pm 0.024\%) \cdot 10^{-15}$  GeV and  $\Gamma = (3.5917 \pm 0.024\%) \cdot 10^{-15}$  GeV. The effect of the mass adjustment in phase space gives an effect of the order of 3%. Agreement with PDG results (see Table 2) is acceptable, but improvements from fits are envisaged.

### 5.3 $K^- \pi^0 K^0 \nu_\tau$

Again, Monte Carlo generated distributions are relegated to the project web page [28]. In particular, successful checks with analytic function for  $d\Gamma/dq^2$  taken from Ref. [25] are shown there. Figure 5 presents comparison between histograms obtained with present and cleo versions of TAUOLA initialization. As we can see, the differences are substantial. Explanations of the previous subsection for the  $K^- \pi^- K^+$  case apply.

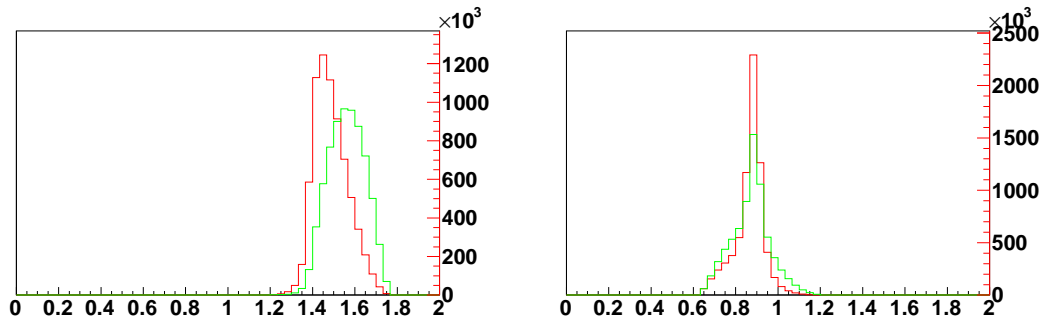


Figure 5: The  $\tau \rightarrow K^- \pi^0 K^0 \nu_\tau$  decay: comparison of distributions for TAUOLA cleo current [14] and for our new current. On the left-hand side, plot of  $K^- \pi^0 K_L^0$  invariant mass is shown and on the right-hand side  $K^- \pi^0$  invariant mass is given. Green histograms (light grey) are for the new current, red (darker grey) are for TAUOLA cleo.

Let us now turn our attention to the partial width for  $K^- \pi^0 K^0$ . The  $SU(2)$  symmetric result from TAUOLA and a sample of  $2 \cdot 10^6$  events,  $(2.7367 \pm 0.025\%) \cdot 10^{-15}$  GeV, agrees well with the analytical result  $(2.7370 \pm 0.02\%) \cdot 10^{-15}$  GeV. The effects of realistic masses in

<sup>23</sup>Whenever possible, the agreement with the data should not be achieved by straightforward violation of the theoretical assumptions. Discrepancies may point to faulty background subtraction, or call for improvements or replacement of the model used in currents calculation. In practice, this may be difficult and require significant and simultaneous effort on both theoretical and experimental sides. That is why one may have to accept temporary introduction of ad-hoc factors into the currents now as well.



phase space are of the order of 1 % and the Monte Carlo result is  $(2.7711 \pm 0.024\%) \cdot 10^{-15}$  GeV. Agreement with the PDG result (see Table 2) is not good.

Analytical results for  $K^-\pi^-K^+$  and  $K^-\pi^0K^0$ , which are obtained in the  $SU(2)$  limit  $\Gamma(\tau^- \rightarrow K^-\pi^-K^+\nu)/\Gamma(\tau^- \rightarrow K^-\pi^0K^0\nu) = 3.7383/2.7370 \simeq 1.366 \simeq 4/3$ , compare well with the result of Ref. [25].

With this subsection, we complete a presentation of results for  $\tau$  decays into three pseudoscalars. Let us now turn to the case of the decays into two pseudoscalars, which are simpler from technical point of view.

#### 5.4 $\pi^-\pi^0\nu_\tau$ , $\pi^0K^-\nu_\tau$ , $\pi^-\bar{K}^0\nu_\tau$ and $K^-K^0\nu_\tau$

In this case, there is only one non-trivial invariant mass distribution,  $d\Gamma/ds$ , which can be constructed from the decay products. This distribution and its ratio to semianalytical result is given for all two pseudoscalar final states in the Web page [28]. For all two-pseudoscalar modes we use samples of  $2 \cdot 10^7$  events<sup>24</sup>.

The analytical result for  $\tau^- \rightarrow \nu_\tau\pi^-\pi^0$  equals  $(5.2431 \pm 0.02\%) \cdot 10^{-13}$  GeV, and for  $\tau^- \rightarrow \nu_\tau K^-K^0$  is  $(2.0863 \pm 0.02\%) \cdot 10^{-15}$  GeV. The Monte Carlo results are respectively  $(5.2441 \pm 0.005\%) \cdot 10^{-13}$  GeV and  $(2.0864 \pm 0.007\%) \cdot 10^{-15}$  GeV. In both channels the physical values of pion and kaon masses are used. As one can see, the obtained  $K^-K^0$  width is only  $\sim 58\%$  of the PDG value. Since the mass of the  $\rho$  resonance is less than the two-kaon threshold, a significant contribution has to be expected from both  $\rho'$  and  $\rho''$ . To check this assumption, we used the parametrization (24) for the two-kaon form factor  $F_{KK}^V$ . For the moment, we use the same numerical value of the parameters  $\gamma$  and  $\delta$  as in the two-pion case, an assumption which holds in the  $SU(3)$  symmetry limit<sup>25</sup>. The result for the partial width of  $\tau^- \rightarrow \nu_\tau K^-K^0$  is  $(2.6502 \pm 0.008\%) \cdot 10^{-15}$  GeV. However, in the real world the parameters for pion and kaon modes are likely not to coincide and have to be fitted by the experiments. Corrections of order  $\sim 30\%$  due to  $SU(3)$  breaking are expected<sup>26</sup>. The Monte Carlo result for the sum of the two channels  $\pi^0K^-\nu_\tau$  and  $\pi^-\bar{K}^0\nu_\tau$  is  $(2.5197 \pm 0.008\%) \cdot 10^{-14}$  GeV if the  $SU(2)$  symmetric masses are used and a sample of  $2 \cdot 10^7$  events is generated with TAUOLA and new currents. The corresponding analytical result is  $(2.5193 \pm 0.02\%) \cdot 10^{-14}$  GeV. The TAUOLA run with physical pion and kaon masses gives  $(2.5092 \pm 0.008\%) \cdot 10^{-14}$  GeV. Separate partial widths for  $\pi^0K^-\nu_\tau$  and  $\pi^-\bar{K}^0\nu_\tau$  channels calculated from the Monte Carlo are given<sup>27</sup> in Table 2. This can be compared<sup>28</sup>

<sup>24</sup>By default, we include the FSI effects, the parameter `FFVEC = 1`. FSI can be switched off if `FFVEC = 0` is set in the file `new-currents/RChL-currents/value_parameter.f`.

<sup>25</sup>The parameters  $\phi_1$  and  $\phi_2$  are subleading and their values are unsubstantial for this check.

<sup>26</sup>For the two-kaon mode one can include a contribution from excited resonances by setting `FFKKVEC = 1`. To run with only  $\rho(770)$  exchange, Eq. (26), set `FFKKVEC = 0`. Our default is `FFKKVEC = 0` and `FFVEC=1`.

<sup>27</sup>To separate submodes one has to set `BRKS = 0` for  $\pi^0K^-$  or `BRKS = 1` for  $\pi^-\bar{K}^0$  in routine `INITDK` residing, e.g., in our example `new-currents/Installation/demo-standalone/taumain.f`.

<sup>28</sup>To run the  $K\pi$  mode with the vector form factor of Eq. (27), `FFKPIVEC = 1` should be set in `new-currents/RChL-currents/value_parameter.f`. To use Eqs. (17) and (18) of Ref. [50] `FFKPIVEC` has to be set to 0. For the default we take `FFKPIVEC = 1`.

with the result  $2.1829 \cdot 10^{-14}$  GeV for the  $K\pi\nu_\tau$  partial width based on Eqs. (17) and (18) of Ref. [50]. The numerical value for parameters of our model are taken from Ref. [50], Table 4, second column. The difference<sup>29</sup> between our and [50] is about<sup>30</sup> 15% for the  $K\pi$  partial width.

In order to test our improvement in the treatment of FSI<sup>31</sup> we have run the program with the FFVEC = 0. It corresponds to neglecting the real part of the loop contributions in  $F_{\pi\pi}^V(s)$ ,  $F_{KK}^V(s)$  and  $F_{K\pi}^V(s)$ , namely  $\text{Re}A_{PQ}(s) = 0$ ,  $\text{Re}A_P(s) = 0$  in Eqs. (24)-(27). In this case, the results for the partial widths are  $\Gamma(\tau^- \rightarrow \nu_\tau \pi^- \pi^0) = (4.0642 \pm 0.005\%) \cdot 10^{-13}$  GeV,  $\Gamma(\tau^- \rightarrow \nu_\tau K^- K^0) = (1.2201 \pm 0.007\%) \cdot 10^{-15}$  GeV (note that only the  $\rho$  meson exchange is included, namely FFKKVEC = 0),  $\Gamma(\tau^- \rightarrow \nu_\tau \pi^0 K^-) = (7.4275 \pm 0.004\%) \cdot 10^{-15}$  GeV,  $\Gamma(\tau^- \rightarrow \nu_\tau \pi^- \bar{K}^0) = (1.4276 \pm 0.006\%) \cdot 10^{-14}$  GeV.

Comparison with the data is technically simpler and further phenomenological efforts should be delegated to that stage of the work. In fits, one has to work with single one-dimensional  $d\Gamma/ds$  spectrum and current as a function of single argument  $s$  as well. We present comparisons of  $d\Gamma/ds$  spectra from cleo current and the present parametrization of TAUOLA, for  $\pi^- \pi^0 \nu_\tau$ ,  $K^- K_S^0 \nu_\tau$  in Fig. 6, and for  $\pi^0 K^- \nu_\tau$  and  $\pi^- K_S^0 \nu_\tau$  in Fig. 7, respectively.

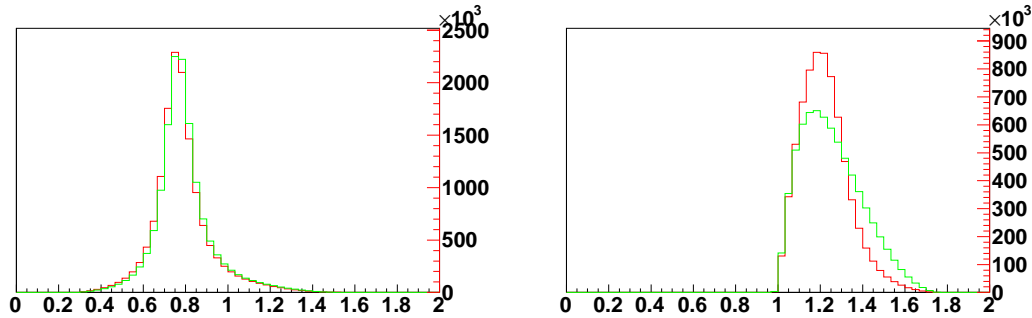


Figure 6:  $\tau \rightarrow \pi^- \pi^0 \nu_\tau$  and  $\tau \rightarrow K^- K_S^0 \nu_\tau$  decays: Comparison of distributions for TAUOLA cleo current [14] and for our new current. On the left-hand side, plot of  $\pi^- \pi^0$  invariant mass is shown and on the right-hand side  $K^- K_S^0$  are for new current, red (darker grey) are for TAUOLA cleo.

## 5.5 Attempt at comparison with the data

Let us stress once again that our parametrization for all new currents is based on Resonance Chiral Theory and is thus self-consistent. However, only minimal attempts on adjusting to the data have been performed. Only one dimensional  $q^2$  distributions have been used

<sup>29</sup>We are thankful to Jorge Portolés for the discussion on the differences between the models.

<sup>30</sup> The reason for this difference of 15% is because we are not using Eq. (19) of Ref. [50]. The difference between the results of Refs. [27] and [50] for the vector form factor contribution is only  $\sim 4\%$ . See Section 7 and Appendix E for a related discussion.

<sup>31</sup>Even a simple Breit-Wigner includes a crude description of FSI [60], where, e.g., off-shell effects are neglected in the resummation of loops.

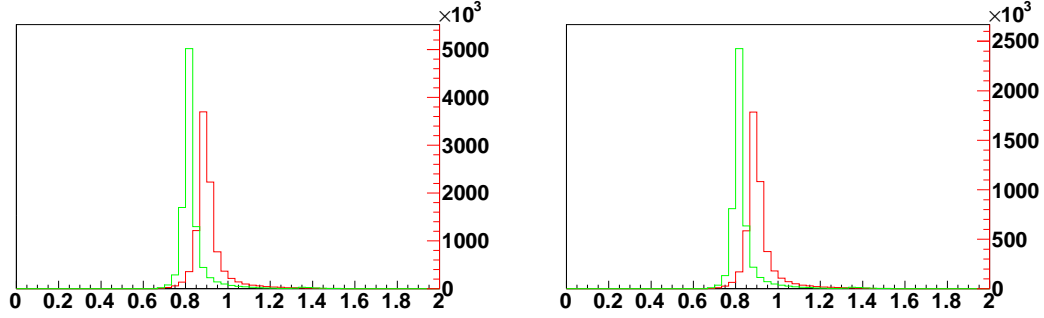


Figure 7:  $\tau \rightarrow \pi^0 K^- \nu_\tau$  and  $\tau \rightarrow \pi^- \bar{K}^0 \nu_\tau$  decays: Comparison of distributions for TAUOLA `cleo` current [14] and for our new current. On the left-hand side, plot of  $\pi^0 K^-$  invariant mass is shown and on the right-hand side  $\pi^- K_S^0$  invariant mass is given. Green histograms (light grey) are for the new current, red (darker grey) are for TAUOLA `cleo`.

in case of  $3\pi$  [24] and  $KK\pi$  [25] decays, to fit parameters such as  $F_V$ ,  $F_A$  etc. For the  $3\pi$  channel, relatively good agreement with ALEPH data is shown in Fig. 3 of Ref. [24], but it represents a consistency check of the input. The proper work on fits is only to start now. The computing and theoretical framework is ready. It is not surprising that, for example, agreement with the unfolded BaBar data, see Fig. 8 of Ref. [61], is not satisfactory.

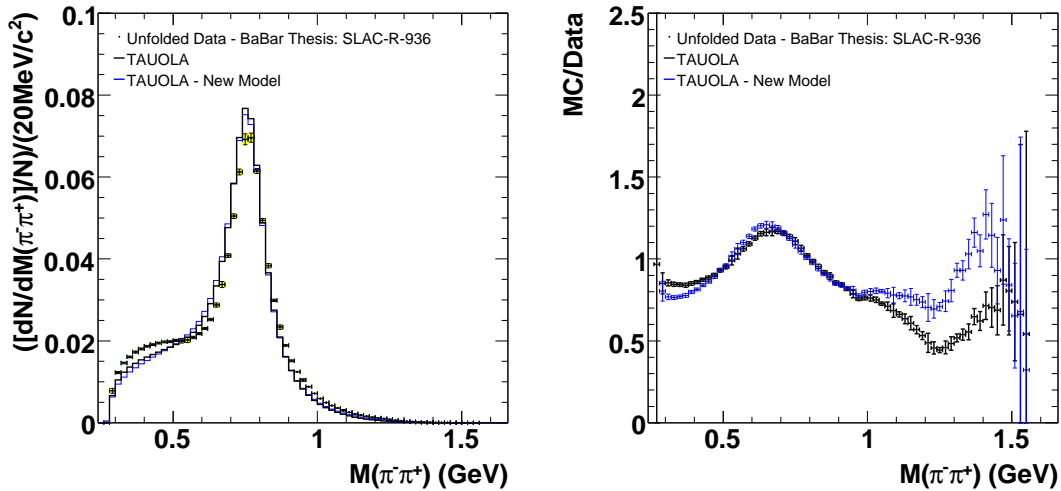


Figure 8: Invariant mass distribution of the  $\pi^+\pi^-$  pair in  $\tau \rightarrow \pi^-\pi^-\pi^+\nu_\tau$  decay. Lighter grey histogram is from our model, darker grey is from default parametrization of TAUOLA `cleo`. The unfolded BaBar data are taken from Ref. [61]. The plot on the left-hand side corresponds to the differential decay distribution, and the one on the right-hand side to plot ratios between Monte Carlo results and data. Courtesy of Ian Nugent.

## 6 Program organization

The reference version of the TAUOLA library that we used as a starting point for the present work is the TAUOLA `cleo` documented in Ref. [14]. The choice is not accidental. This version is used as a starting point for Belle and BaBar software as well. Also C++ implementation of TAUOLA [62], installed in the library of Ref. [63], uses this initialization. Porting into collaboration software is thus technically prepared. This means the solution will be convenient for many users.

Hadronic current represents a rather compact segment of the simulation package. That is why only minor changes need to be introduced to TAUOLA `cleo` code and the makefile. Only several lines will be necessary to modify in the collaboration software. All the rest is included in `tar-ball` to be expanded in `tauola` directory. See Appendix B for details.

The user will be able to switch to the new current invoking simply `CALL INIRChL(1)` prior to TAUOLA initialization, still retaining possibility to use the old ones with `CALL INIRChL(0)` as well.

An algorithm for working with auxiliary weights to implement simultaneously several models of  $\tau$  decays is a straightforward extension.

### 6.1 Weight recalculation

Present day experimental data feature very high precision over all directions of multidimensional phase space. Nonetheless cross contamination between different channels takes place. This is the case, for example, if particular decay channels differ by presence or absence of  $\pi^0$ 's. Figure 6 of Ref. [6] represents such folded comparison between data and Monte Carlo for the  $\tau^+ \rightarrow \pi^+\pi^0\bar{\nu}_\tau$  decay channel. This result can not be used, without additional information on other decay channels, for fits of hadronic current. This takes place even for this seemingly simple case where hadronic current can be directly deciphered from a one-dimensional distribution.

In general, for the precision matching of data and models it is convenient to simultaneously confront several models and take into consideration all decay channels simultaneously. Such a solution may be a necessary technical step if fits for unfolded data are envisaged at the precision level better than few percents.

To facilitate technical tasks, a weight recalculation method is prepared, following discussions and recommendations given in Ref. [9]. It was agreed that organization of the programs should enable simulation following the scheme of Fig. 9. For the single generated Monte Carlo sample (when all detector and experimental acceptance effects are taken into account), one can calculate weights enumerating change of matrix element. The procedure can be repeated as many times as needed. In this way the optimal choice is met when all experimental and theoretical effects can be taken into account. With this, the fit to multidimensional distribution of measured data can be determined.

We have prepared the necessary changes for TAUOLA. The following algorithm was checked to work (its technical details are given in Appendix B.4):

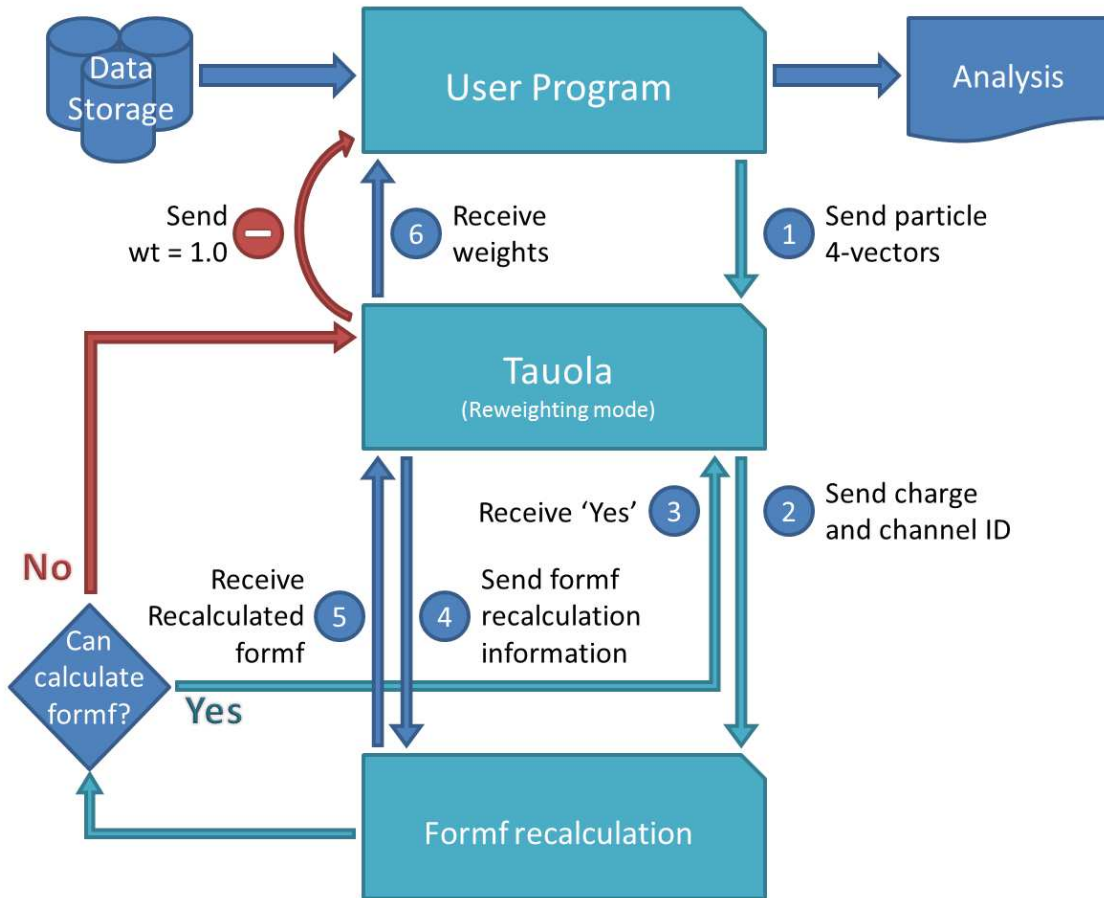


Figure 9: Weight recalculation model, as discussed in Ref. [64].

1. For each generated  $\tau$  stored in a datafile, the user program reads flavours and 4-vectors of  $\tau$  and its decay products.
2. Appropriate kinematic transformation is performed enabling a recalculation of the matrix element, exactly as at the generation step.
3. An appropriate routine of TAUOLA is chosen and the matrix element is calculated.
4. Another instance of TAUOLA initialization can be activated and the matrix element recalculated using a different physics model.
5. If one of the two models was used in the generation of the user sample, then the weight for model replacement can be calculated as a simple ratio of the two.

Usage of this method of weight recalculation does not require any changes to TAUOLA code except those related to installation of the presented upgrade, aiming at installation of our new RChL currents. Needless to say, the method can be used several times for user variants of RChL and interpolation of weights can be used in fits. In our example, given in directory `new-currents/Installation-Reweight` we provide a simple method to read generated events from file, but it can be easily adapted to any other one. Linking libraries of MC-TESTER, ROOT or HepMC is an option convenient also for an interpretation/verification of results.

Basic features which are necessary for our solution have already been tested for Belle and BaBar software environments. Changes presented in Appendix B are from that perspective rather straightforward.

## 7 Theoretical basis of the currents

### 7.1 Resonance Chiral Theory framework

The Lorentz structures of currents are universal and a proper minimal set of form factors only needs to be chosen for a particular decay mode. One can recall the QCD symmetries to gain some insight in the form factors. It is particularly useful that the chiral symmetry of massless QCD allows one to develop an effective field theory description,  $\chi PT$ , valid for momenta much smaller than the  $\rho$  mass [19, 20]. However,  $\chi PT$  cannot provide predictions valid all over the  $\tau$  decay phase space [65], it constrains nonetheless the form and normalization of the form factors in such limit<sup>32</sup>.

The computations done within Resonance Chiral Theory ( $R\chi T$  [22, 23]) are able to reproduce the low-energy limit of  $\chi PT$  up to  $NLO$ <sup>33</sup> and demonstrate the right falloff [67, 68] in the high energy region. The current state-of-the-art for the hadronic  $\tau$  decays form factors ( $F_i$ ) is described in Refs. [49, 69].

The description provided by  $R\chi T$  complies with the low-energy properties of the underlying theory, at least up to next-to-leading order<sup>34</sup>. Nonetheless it is necessary to extend  $\chi PT$  to the intermediate energy region, which is probed through hadronic  $\tau$  decays. In order to do this, one relies on the large- $N_C$  expansion of QCD [73, 74, 75] which predicts that in the  $N_C \rightarrow \infty$  limit there is an infinite tower of zero-width resonances experiencing among them local effective interactions taken at tree level. We model this setting with a spectrum that resembles the measured one<sup>35</sup>. We introduce a  $NLO$  effect (whose impact is, however, quite sizable in phenomenological applications) in that counting, providing the

---

<sup>32</sup>One should keep in mind that the effect due to different and nonzero masses of  $u$  and  $d$  quarks already now seems to be necessary to explain some aspects of  $\tau$  data.

<sup>33</sup>The improvement obtained when doing this can be appreciated in Fig. 1 of Ref. [66].

<sup>34</sup>Also the leading next-to-next-to-leading (NNLO) order terms [70, 71] are reproduced [51, 72].

<sup>35</sup>In  $R\chi T$  all nine mesons [ $\rho$ ,  $K^*$ ,  $\omega$ , ( $\phi$ )] have the same mass in the  $N_C \rightarrow \infty$  limit without taking into account  $SU(3)$  breaking. The  $1/N_C$  corrections make the  $\phi$  heavier [through the axial anomaly that breaks  $U(3)$  down to  $SU(3)$ ].  $SU(3)$  breaking makes  $M_\rho \neq M_{K^*} \neq M_\omega$ .

resonances with an energy-dependent width computed<sup>36</sup> within  $R\chi T$  (see Section 3).

The appropriate falloff at large energies [67, 68] is imposed to the form factors, vector-vector and axial-vector—axial-vector correlators [46, 76, 77, 78, 79]. This results in a set of relations among the coupling constants of the theory, which are obtained working in the single resonance approximation (only the lightest multiplet of resonances is included per given set of quantum numbers) and in the  $N_C \rightarrow \infty$  limit. Upon integration of the resonances, this procedure allows the saturation of the values of the  $\chi PT$  low-energy constants at  $\mathcal{O}(p^4)$  and  $\mathcal{O}(p^6)$ , both in the even- and odd-intrinsic parity sectors.

The results for all hadronic currents have been calculated within  $R\chi T$  working, with the exception of both two-pion and two-kaon modes, in the isospin limit. Therefore the corresponding hadronic form factors depend only on the average pion and kaon masses:

$$m_\pi = (m_{\pi^0} + 2 \cdot m_{\pi^+})/3, \quad m_K = (m_{K^0} + m_{K^+})/2. \quad (42)$$

For the three-pseudoscalar modes every hadronic form factor consists of 3 parts: a chiral contribution (direct decay, without production of any intermediate resonance), one-resonance and double-resonance mediated processes. The precise form of the form factors for three-pion and (two pions - one kaon) modes is presented in Sections 2.1, 2.2 and 2.3. For the two-meson modes the corresponding vector form factors are built from the lightest resonance contribution in  $R\chi T$  [51]. FSI are resummed by means of an Omnès function [51], see Section 2.4. Both two- and three-meson  $\tau$  decays are sensitive to the exchange of excited resonances, whose contribution we have to account for. The exchange of heavier-resonances could be computed in the same fashion as for the lightest multiplet, giving rise to new unknown couplings<sup>37</sup>. This possibility has been postponed for the moment to prevent the increase in the number of free parameters. We believe that it is sensible to tackle this task once more knowledge on the couplings of the  $R\chi T$  is achieved. In the three-meson decays, the excited resonances have been included phenomenologically, introducing an additional parameter,  $\beta_{\rho'}$ , in Eq. (11). This has been done in such a way to keep the chiral limit result and the QCD-ruled short-distance behaviour. For the two-meson processes, they have been included analogously as the lightest resonance contribution, making sure that the appropriate low- and high-energy limits are not spoiled and that unitarity and analyticity hold perturbatively<sup>38</sup>. Following the approximation proposed in Ref. [53], three new parameters, related with the  $\rho(1450)$ ,  $\rho(1700)$  and  $K^{*'}(1410)$  couplings, appear:  $\gamma \equiv -F'_V G'_V / F^2$  [for  $\rho(1450)$ ],  $\delta \equiv -F''_V G''_V / F^2$  [for  $\rho(1700)$ ] and  $\gamma_{K\pi} \equiv -F'_V G'_V / (F F_K)$  [for  $K^{*'}(1410)$ ]<sup>39</sup> in Eqs. (24) and (27). The short-distance QCD constraint for the vector form factor will require the relation  $F_V G_V + F'_V G'_V + F''_V G''_V + \dots = F^2$  to hold.

---

<sup>36</sup>The width of a spin-one resonance is defined [52] as the imaginary part of the pole generated by resumming those diagrams, with an absorptive part in the s-channel, that contribute to the two-point function of the corresponding vector current.

<sup>37</sup>See, for instance Refs. [80, 81].

<sup>38</sup>See subsection 7.3 points 1 and 3 and Appendix E for an improved treatment.

<sup>39</sup>Due to SU(3) breaking effects  $\gamma \neq \gamma_{K\pi}$ .

## 7.2 The error associated to the $1/N_C$ expansion

Any model based on the  $1/N_C$  expansion will naturally raise the question of the error associated to that expansion, which can be naively estimated as  $1/N_C \sim 30\%$ . It is natural to object to the convergence of a series in  $1/N_C$  that ends up being  $1/3$  in the real world. The associated error of the size of the expansion parameter would be much larger than the statistical error of experimental measurements or even of our precision target of a few percent. Just to give a counterexample, a look at the results of Ref. [51] will quickly suggest that the actual error can be much smaller, which is noteworthy, especially taking into account that in the quoted reference, an impressive agreement with data in  $e^+e^- \rightarrow \pi^+\pi^-$  up to  $s = 1 \text{ GeV}^2$  was obtained in terms of just one parameter,  $M_\rho$ .

Let us recall how this can be possible. First, the large- $N_C$  expansion of QCD is not an expansion in the usual perturbative sense. For instance, in QED, the perturbative expansion means, firstly, that the diagrams with less photon couplings to fermionic lines dominate. After that, when we compute diagrams both at tree level, and including loops, we realize that the expansion parameter is  $\alpha = e^2/(4\pi)^2$  and the coefficients of the series are small compared to  $\alpha$ : every order we go further in the expansion the error reduces by  $\sim 1/\alpha \simeq 137$ . In the large- $N_C$  expansion of QCD, we know first, which diagrams are leading-order (planar diagrams with gluon exchanges) and which ones are suppressed. Unfortunately, the expansion has a fundamental subtlety that prevents one from determining the expansion parameter after that: there are infinite diagrams at any given order in the expansion, so that one cannot perform a calculation at both LO and NLO and compare them to know what is the expansion parameter. It is known, however, that diagrams with internal quark loops are suppressed as  $1/N_C$  and that non-planar diagrams are suppressed as  $1/N_C^2$ . Moreover, if the number of quark flavours,  $n_f$ , is not considered to be smaller than  $N_C$  the former diagrams can even scale as  $n_f/N_C$ . These kind of contributions would be responsible for the mixing of  $q\bar{q}$  and  $q\bar{q}q\bar{q}$  states. The fact that this effect is not observed in Nature and the success of the quark model classification of mesons in  $q\bar{q}$  multiplets suggests that the coefficients of these diagrams with internal quark loops are tiny, in such a way that the first non-negligible correction would come from the non-planar diagrams, suppressed as  $1/N_C^2 \sim 10\%$ . This reasoning may explain why the large- $N_C$  expansion is a such a good approximation for low and intermediate-energy QCD, given the phenomenological successes of its applications in meson effective field theories [82] and the corroborated predictions given by the large- $N_C$  limit both for  $\chi PT$  [83, 84] and for  $R\chi T$  [23] coupling constants. All these reasons seem to suggest that, quite generally, some factor comes to complement  $1/N_C$  for the value of the expansion parameter to be reduced and the relative accuracy to be increased.

This conclusion is supported by the investigation of some  $\mathcal{O}(p^4)$  and  $\mathcal{O}(p^6)$  couplings of  $\chi PT$ , which are done modelling the NLO expansion in  $1/N_C$  of  $R\chi T$  [85, 86, 87, 88, 89]. According to the size of the corrections, we judge that 15% can be a reasonable general estimate (see, however, our discussion in Appendix C on the possible variations on the predictions of the couplings obtained in the  $N_C \rightarrow \infty$  limit). Noticeably, the actual expansion parameter can be computed for  $R\chi T$  in the study of the vector form factor of



the pion at  $NLO$  in the  $1/N_C$  expansion [90], yielding

$$\alpha_V = \frac{n_f}{2} \frac{2G_V^2}{F^2} \frac{M_V^2}{96\pi F^2}, \quad (43)$$

which, at lowest order, is the ratio of the vector width and mass,  $\alpha_V \sim 0.2$ , agreeing with the previous discussion.

Moreover, we should emphasize that our approach goes beyond the  $N_c \rightarrow \infty$  limit. We supplement the lowest order in the  $1/N_C$  expansion for the theory in terms of mesons by the leading higher-order correction, namely by including the resonance (off-shell) widths for the wide states  $\rho$ ,  $K^*$  and  $a_1$ . This seems to point to smaller errors than those characteristic of the  $LO$  contribution in the  $1/N_C$  expansion and may be able to explain, altogether, an eventual fine agreement with data.

### 7.3 Other sources of error

Once this major concern on the reliability of the  $R\chi T$  hadronic currents has been discussed, let us consider in turn other possible sources of error in the different hadronic  $\tau$  decay modes considered.

1. In the two-meson  $\tau$  decay modes an Omnès type of resummation is employed for the FSI. The proposed expressions, Eqs. (24) to (27), respect unitarity and analyticity only in a perturbative sense (this will be improved along the lines discussed in Appendix E). The effect of these violations is, however, pretty small, as one can see comparing the results of Refs. [27] and [50] for the  $\tau \rightarrow K\pi\nu_\tau$  decays. That is why we consider our current parametrizations for these decay channels a reasonable temporary approach. For a future update of the program we recall that Eqs. (24) to (27) should be replaced, using the procedure described in Appendix E. For the  $K\pi$  vector form factor we are going to use<sup>40</sup> the parametrization of Ref. [50] in a future upgrade of the program. Analogous works for the  $\pi^-\pi^0$  and  $K^-K^0$  vector form factors are under way.
2. In the three-meson modes, scalar and pseudoscalar resonance exchange has been neglected. The spin-one character of the SM couplings of the hadron matrix elements in the  $\tau$  decays implies that the form factors for these processes are ruled by vector and axial-vector resonances. Their contribution should be minor in  $\tau \rightarrow KK\pi\nu_\tau$  decays (see the related discussion in Section 2 of Ref. [25]) while that of the scalar resonances can be a bit more important in  $\tau \rightarrow 3\pi\nu_\tau$  decays. The lightest scalars are, however, suppressed in the large- $N_C$  limit (see, however, Ref. [92]). In these decays, we have also neglected systematically three-body FSI for the moment. They may be important in the available phase space and at the required precision [93, 94], thus, should

---

<sup>40</sup>We note that another interesting approach, based on Omnès integral equations incorporating both chiral constraints at low energies and QCD short-distance relations at high energies was performed in Ref. [91]; isospin-violating corrections were also studied.

be investigated at a time of comparison to experimental data. The present step of our work is devoted predominantly to establish a technical environment. Consequently, the effort was concentrated on those theoretical aspects which bring difficulties in program design and a careful discussion of potentially less important effects is delegated to the future work. Finally, the computation of  $\Gamma_{a_1}(q^2)$  through the optical theorem [24] does not give the corresponding real part of the loop function, which we have disregarded. Although this approximation might be supported numerically it induces a small violation of analyticity.

3. In the  $\tau \rightarrow KK\pi\nu_\tau$  decays, for the moment, we have not included the contribution of excited resonances. We expect that their influence is bigger in this case than in the three-pion channels, since the mass of the hadronic system is larger. The impact of this error can be as large as the one coming from the  $1/N_C$  expansion.

## 7.4 Numerical estimates of the errors in the different decay channels and distributions

What is the numerical precision we should expect in confrontation of our currents with the data? As already mentioned, a first crude estimation gave us an error of the order of the expansion parameter,  $1/N_C$ , thus 30% precision tag for our results, but we already accumulated, during the preceding discussion, a number of indications pointing to better accuracy of the results obtained within this approach. It is thus of importance [95] to evaluate solely on the basis of theoretical considerations, for which decay channels we expect precision to be better or worse and in which regions of the phase space. This is of course a must for scientific theory as Resonance Chiral Theory is supposed to be.

The answer, if scientific theory holds, always comes from the confrontation with the data. Results from theory have to be prepared in such a manner that agreement confirms and discrepancy invalidates the theory under consideration. Theoretical results have to include estimation of their errors from within theory itself. That is the basic principle of science methodology and our work has to keep this aspect in mind too. We have to address what is input and where such confrontation may take place.

Until now we see that the precision can be at the level of a few percent<sup>41</sup> for the two-meson modes [6, 27, 49, 50, 53, 96]. Despite the accuracy is at a comparable level for the  $d\Gamma/dq^2$  distributions in the three-pion decays, the error on the distribution in the  $\pi^+\pi^-$  invariant mass is at the level of  $\sim 20\%$ . We expect to improve it to a few percent level once FSI are accounted for. In the  $\tau \rightarrow KK\pi\nu_\tau$  decays the situation is, somehow, reversed. The largest error ( $\sim 30\%$ ) comes on the  $d\Gamma/dq^2$  distribution, while the accuracy is much better in the  $K^+\pi^-$  ( $\sim 10\%$ ) and  $K^+K^-$  ( $\sim 5\%$ ) distributions. We expect that the errors on the  $KK\pi$  modes are reduced a factor of two when the excited resonances contributions will be taken into account.

---

<sup>41</sup>Once the parameters entering Eq.(26) are fitted, we expect similar accuracy for the  $KK$  modes as in the  $\pi\pi$  and  $K\pi$  cases.

To get form factors with substantially better agreement with the data, one may need to introduce ad-hoc factors, hopefully close to unity and hopefully based on educated guesses. This may provide a valuable hint for future theoretical work.

## 8 Summary

In this paper we have documented a set of currents based on Resonance Chiral Theory for use in hadronic  $\tau$  decays into either two ( $\pi^-\pi^0$ ,  $\pi^0K^-$ ,  $\pi^-\bar{K}^0$  and  $K^-K^0$ ) or three ( $\pi^-\pi^-\pi^+$ ,  $\pi^0\pi^0\pi^-$ ,  $K^-\pi^-K^+$ ,  $K^0\pi^-\bar{K}^0$  and  $K^-\pi^0K^0$ ) pseudoscalars. The set covers more than 88% of total hadronic  $\tau$  width. Technical tests of the installation into the FORTRAN program have been documented. The set can be used as an upgrade easy to install into any version of the TAUOLA  $\tau$  decay library. In this way currents are ready for confronting the  $\tau$  decay data (unfolded or not). Precision fits can be performed and arrangements for use of model-dependent weights are ready for that purpose.

On the technical side, the  $\tau$  decay algorithms themselves have been checked down to 0.05% precision level. To this end, a detailed comparison between analytic and Monte Carlo results has been provided. Statistical samples, 2 (3) orders of magnitude larger than at time of reference [14] ([11]) were used. This technical precision of 0.05% is substantially better than physics precision of our currents which we estimate at the 5-30% level, depending on the channel. Software environment for further phenomenological work is prepared.

In the present work, we have concentrated on decay modes contributing to 88% of the  $\tau$  hadronic decay width. In particular, the decay modes of  $\tau$  into  $4\pi$ 's have not been updated in our work. The currents for these decays, constructed on the basis of low-energy  $e^+e^- \rightarrow$  hadrons data have been available since Ref. [33]. For the time being this can be used as an alternative to TAUOLA c1eo default of Ref. [14] in discussion of the systematic error for background modelling. In these decay modes theoretical foundations are less profound, but we hope that the presented solution will not jeopardize analysis of other channels due to lesser control of cross contaminating channels. Together with  $4\pi$ 's currents described in Ref. [33] our system covers now 97% of the total hadronic  $\tau$  width.

It is straightforward to extend our work to more elaborated currents including, e.g. scalar form factors. Because of different nature of benchmark distributions, technical aspects and different physics assumptions we leave this task to the forthcoming work [29].

As a consequence of comparisons with the data, some of the theoretical assumptions may need to be reconsidered too. We start from a theoretical approach common for all channels. Empiric form factors may need to be added later though. In this way not only agreement with the data will be established, but eventual inefficiencies of our starting approach will be numerically evaluated. That is why, it is important to ensure that model-dependent weights can be calculated after (and independently of) the detector effects. There are several assumptions which lie behind our calculations and in case of discrepancy with the data they may need to be revisited. Let us list them in descending order of their theoretical foundation:

1. We assume that Lorentz invariance will not need to be reconsidered at any step of

our project.

2. With respect to the separation of the matrix element into leptonic and hadronic parts, we assume that electroweak corrections will not affect such separation beyond precision level of several permille at most, the question of an overall normalization factor for all hadronic channel, see e.g. Refs. [97, 98, 99], is of no practical importance for Monte Carlo.
3. We assume that isospin symmetry should be a good guiding principle. We suppose that it should hold more accurately for distributions than for amplitude phases, but we do not expect large effects.
4. Some of the effective couplings can be predicted by considering the asymptotic behaviour of Green functions and form factors both in the effective theory ( $R\chi T$ ) and in the operator product expansion of QCD [23]. However, these predictions are affected by different sources of errors, most importantly the model dependence on the realization of the large- $N_C$  limit of QCD [100, 101, 102, 103, 104, 105, 106, 107] (mainly the choice of the resonance spectra, but not only). Special care should be taken when relating different channels, especially if the statistics in both of them is very different and in one decay channel only a subset of resonance parameters is used. One should not forget that the (formal or not) integration of heavy degrees of freedom out of the action affects the values of the parameters in the remaining lower-energy theory. Results for the individual modes should be analyzed consequently.
5. Our effective couplings and interactions are based on the low-energy effective field theory of QCD ( $\chi PT$ ), whose results are reproduced at NLO in the corresponding limit by  $R\chi T$ . Although the latter being formally sound, there is model dependence in any realization of the large- $N_C$  limit of QCD for mesons and, moreover, we are introducing the contribution of excited resonances only at a phenomenological level, see Eq. (11) and the related discussion in Section 7, a feature that can be improved in the future. We may need to explore the limits of such approach and take feed back from experiments.
6. Different solutions have been advocated for taking unitarity properties, via the propagator widths, into account. In particular, there is no consensus that the exponentiation of the real part of the resonance width is always the best solution. This point must be investigated further, especially in light of precision fits to high-statistics data.

At the same time, the seeming violation of these principles may be a consequence of some experimental problems. That is why such discussion requires simultaneous participation of theorists and experimental physicists and the proper software environment.

Such fine-tunings took place for TAUOLA version of Ref. [11]. The improved agreement with the data of CLEO and ALEPH has been achieved thanks to the effort of these collaborations resulting with TAUOLA `cleo` and TAUOLA `aleph` initializations. The code is

available from Ref. [14]. We should expect similar work with our present parametrizations. We hope that, in this way, theoretical and experimental constraints will be appropriately matched leading to a representation of experimental and theoretical achievements in common language of value for future research. Once such confrontation with the Belle or BaBar data is completed, one will profit from the technical precision of the simulation established here and thanks to prepared flexibility for FORTRAN [14] and C++ [62] users of high-energy experiments such as at LHC or for LC will benefit as well. If analytic form of the form factors will be attained, it may help start future work for such research as lattice calculations.

We consider this work as a step towards a theoretically rigorous description of hadronic tau decay data but, at this moment, we can still not be sure that the currents for all channels will be able, after fits, to describe all data well. In this case, detailed numerical information on the offending distributions will be provided. Further theoretical work is stimulated. Some intermediate results are presented in [108, 109, 110].

## Acknowledgements

Our project is coordinated with the effort of the Working Group on Radiative Corrections and MC Generators for Low Energies (<http://www.lnf.infn.it/wg/sighad/>). Useful discussions and help in understanding requirements our extensions must fulfil to be useful for BaBar and Belle go to John Michael Roney, Simon Eidelman and Hisaki Hayashii. We are thankful to Ian M. Nugent and Denis Epifanov for comments on the document and our program installation procedure. Thanks to Kenji Inami for help in organization of tests within Belle collaboration environment and to Swagato Banerjee for discussions as well.

We would like to thank Jorge Portolés for fruitful discussions on the hadronic form factors and currents. We are thankful to Matthias Jamin, Diogo Boito and Rafel Escribano for discussions of the  $K\pi$  vector form factor. We are indebted to Johann Hans Kühn for discussions and critical concerns important for the present and future steps of the project.

We acknowledge the inspiring environment of Stefano Bellucci's group at LNF, (INFN, Frascati), where important step of the project was achieved. This research of OS was supported by a Marie Curie Intra European Fellowship within the -7th European Community Framework Programme (FP7-PEOPLE-2009-IEF) PIEF-GA-2009-253329 and by the Spanish Consolider Ingenio 2010 Programme CPAN (CSD2007-00042) as well by by MEC (Spain) under Grants FPA2007-60323, FPA2011-23778. The work of PR has been supported in part by MEC (Spain) under Grants FPA2007-60323, FPA2008-01430, FPA2011-23778, FPA2011-25948 and by the Spanish Consolider Ingenio 2010 Programme CPAN (CSD2007-00042). The work of ZW is supported in part by the Polish Ministry of Science and Higher Education grant No. 1289/B/H03/2009/37 and of TP by the Polish Government grant NN202127937 (years 2009-2011) under decision DEC-2011/03/B/ST2/00107. From January 1, 2013, the affiliation of O. S. is IFJ PAN, Krakow, Poland.

## References

- [1] E. Braaten, S. Narison, and A. Pich, *Nucl.Phys.* **B373** (1992) 581.
- [2] E. Braaten, *Phys.Rev.* **D39** (1989) 1458.
- [3] E. Braaten, *Phys.Rev.Lett.* **60** (1988) 1606.
- [4] S. Narison and A. Pich, *Phys.Lett.* **B211** (1988) 183.
- [5] A. Pich, *Conf.Proc.* **C890523** (1989) 416.
- [6] Belle Collaboration, M. Fujikawa *et al.*, *Phys. Rev.* **D78** (2008) 072006, 0805.3773.
- [7] Z. Dolezal, *PoS HQL2010* (2010) 079.
- [8] M. Rama, *Nucl.Phys.Proc.Suppl.* **210-211** (2011) 199.
- [9] Working Group on Radiative Corrections and Monte Carlo Generators for Low Energies Collaboration, S. Actis *et al.*, *Eur.Phys.J.* **C66** (2010) 585, 0912.0749.
- [10] Belle Collaboration, H. Hayashii and M. Fujikawa, *Nucl.Phys.Proc.Suppl.* **198** (2010) 157.
- [11] S. Jadach, Z. Was, R. Decker, and J. H. Kühn, *Comput. Phys. Commun.* **76** (1993) 361.
- [12] J. H. Kuhn and A. Santamaría, *Z. Phys.* **C48** (1990) 445.
- [13] J. H. Kuhn and E. Mirkes, *Z. Phys.* **C56** (1992) 661.
- [14] P. Golonka *et al.*, *Comput. Phys. Commun.* **174** (2006) 818, hep-ph/0312240.
- [15] R. Decker, M. Finkemeier, and E. Mirkes, *Phys. Rev.* **D50** (1994) 6863, hep-ph/9310270.
- [16] R. Decker, E. Mirkes, R. Sauer, and Z. Was, *Z. Phys.* **C58** (1993) 445.
- [17] D. Gómez Dumm, A. Pich, and J. Portolés, *Phys. Rev.* **D69** (2004) 073002, hep-ph/0312183.
- [18] S. Weinberg, *Physica* **A96** (1979) 327, Festschrift honoring Julian Schwinger on his 60th birthday.
- [19] J. Gasser and H. Leutwyler, *Ann. Phys.* **158** (1984) 142.
- [20] J. Gasser and H. Leutwyler, *Nucl. Phys.* **B250** (1985) 465.
- [21] CLEO Collaboration, T. Coan *et al.*, *Phys.Rev.Lett.* **92** (2004) 232001, hep-ex/0401005.

- [22] G. Ecker, J. Gasser, H. Leutwyler, A. Pich, and E. de Rafael, *Phys. Lett.* **B223** (1989) 425.
- [23] G. Ecker, J. Gasser, A. Pich, and E. de Rafael, *Nucl. Phys.* **B321** (1989) 311.
- [24] D. G. Dumm, P. Roig, A. Pich, and J. Portolés, *Phys. Lett.* **B685** (2010) 158, 0911.4436.
- [25] D. G. Dumm, P. Roig, A. Pich, and J. Portolés, *Phys. Rev.* **D81** (2010) 034031, 0911.2640.
- [26] E. Arganda, M. J. Herrero, and J. Portolés, *JHEP* **06** (2008) 079, 0803.2039.
- [27] M. Jamin, A. Pich, and J. Portolés, *Phys.Lett.* **B664** (2008) 78, 0803.1786.
- [28] T. Przedzinski, O. Shekhovtsova, and Z. Was, <http://annapurna.ifj.edu.pl/~wasm/RChL/RChL.htm> or “Projects 2011/12” on <http://wasm.home.cern.ch/~wasm/>.
- [29] O. Shekhovtsova *et al.*, in preparation.
- [30] J. Gasser and H. Leutwyler, *Nucl.Phys.* **B250** (1985) 517.
- [31] Particle Data Group Collaboration, K. Nakamura, *J. Phys.* **G37** (2010) 075021.
- [32] A. Pich, *Phys.Lett.* **B196** (1987) 561.
- [33] A. E. Bondar *et al.*, *Comput. Phys. Commun.* **146** (2002) 139, hep-ph/0201149.
- [34] E. Barberio and Z. Was, *Comput.Phys.Commun.* **79** (1994) 291–308.
- [35] N. Davidson, T. Przedzinski, and Z. Was, 1011.0937.
- [36] V. Cirigliano, G. Ecker, and H. Neufeld, *Phys.Lett.* **B513** (2001) 361, hep-ph/0104267.
- [37] V. Cirigliano, G. Ecker, and H. Neufeld, *JHEP* **0208** (2002) 002, hep-ph/0207310.
- [38] F. Flores-Báez, A. Flores-Tlalpa, G. López Castro, and G. Toledo Sánchez, *Phys.Rev.* **D74** (2006) 071301, hep-ph/0608084.
- [39] Z.-H. Guo and P. Roig, *Phys.Rev.* **D82** (2010) 113016, 1009.2542.
- [40] G. Nanava and Z. Was, *Eur.Phys.J.* **C51** (2007) 569, hep-ph/0607019.
- [41] G. Nanava, Q. Xu, and Z. Was, *Eur.Phys.J.* **C70** (2010) 673, 0906.4052.
- [42] Q. Xu and Z. Was, 1201.0189.
- [43] G. Kramer, W. F. Palmer, and S. S. Pinsky, *Phys. Rev.* **D30** (1984) 89.

- [44] J. Wess and B. Zumino, *Phys.Lett.* **B37** (1971) 95.
- [45] E. Witten, *Nucl.Phys.* **B223** (1983) 422.
- [46] P. Ruiz-Femenía, A. Pich, and J. Portolés, *JHEP* **0307** (2003) 003, hep-ph/0306157.
- [47] BABAR Collaboration Collaboration, B. Aubert *et al.*, *Phys.Rev.Lett.* **100** (2008) 011801, 0707.2981.
- [48] Belle Collaboration Collaboration, K. Inami *et al.*, *Phys.Lett.* **B643** (2006) 5–10, hep-ex/0609018.
- [49] P. Roig, 1112.0962.
- [50] D. R. Boito, R. Escribano, and M. Jamin, *Eur. Phys. J.* **C59** (2009) 821, 0807.4883.
- [51] F. Guerrero and A. Pich, *Phys.Lett.* **B412** (1997) 382–388, hep-ph/9707347.
- [52] D. Gómez Dumm, A. Pich, and J. Portolés, *Phys. Rev.* **D62** (2000) 054014, hep-ph/0003320.
- [53] M. Jamin, A. Pich, and J. Portolés, *Phys.Lett.* **B640** (2006) 176, hep-ph/0605096.
- [54] S. Jadach, J. H. Kühn, and Z. Wąs, *Comput. Phys. Commun.* **64** (1990) 275.
- [55] <http://wwwasdoc.web.cern.ch/wwwasdoc/cernlib.html>.
- [56] G. Lepage, *J.Comput.Phys.* **27** (1978) 192, Revised version.
- [57] N. Davidson, P. Golonka, T. Przedzinski, and Z. Was, *Comput.Phys.Commun.* **182** (2011) 779, 0812.3215.
- [58] CLEO Collaboration, F. Liu, *Nucl.Phys.Proc.Suppl.* **123** (2002) TU07, hep-ex/0209025.
- [59] J. Portolés, *Nucl.Phys.Proc.Suppl.* **144** (2005) 3, hep-ph/0411333.
- [60] M. Jamin, J. A. Oller, and A. Pich, *Nucl.Phys.* **B622** (2002) 279–308, hep-ph/0110193.
- [61] I. M. Nugent, SLAC-R-936, Ph.D. Thesis.
- [62] N. Davidson, G. Nanava, T. Przedzinski, E. Richter-Was, and Z. Was, *Comput.Phys.Commun.* **183** (2012) 821, 1002.0543.
- [63] M. Kirsanov, A. Ribon, and O. Zenin, *PoS ACAT08* (2008) 114.
- [64] Z. Was, *Nucl.Phys.Proc.Suppl.* **218** (2011) 249, 1101.1652.



- [65] G. Colangelo, M. Finkemeier, and R. Urech, *Phys.Rev.* **D54** (1996) 4403, [hep-ph/9604279](#).
- [66] P. Roig, *Nucl.Phys.Proc.Suppl.* **189** (2009) 78, [0810.5764](#).
- [67] S. J. Brodsky and G. R. Farrar, *Phys. Rev. Lett.* **31** (1973) 1153.
- [68] G. P. Lepage and S. J. Brodsky, *Phys. Rev.* **D22** (1980) 2157.
- [69] J. Portolés, *AIP Conf.Proc.* **1322** (2010) 178, [1010.3360](#).
- [70] J. Bijnens, G. Colangelo, and P. Talavera, *JHEP* **9805** (1998) 014, [hep-ph/9805389](#).
- [71] J. Bijnens and P. Talavera, *JHEP* **0203** (2002) 046, [hep-ph/0203049](#).
- [72] F. Guerrero, *Phys.Rev.* **D57** (1998) 4136–4141, [hep-ph/9801305](#).
- [73] G. 't Hooft, *Nucl.Phys.* **B72** (1974) 461.
- [74] G. 't Hooft, *Nucl.Phys.* **B75** (1974) 461.
- [75] E. Witten, *Nucl.Phys.* **B160** (1979) 57.
- [76] V. Cirigliano, G. Ecker, M. Eidemuller, A. Pich, and J. Portolés, *Phys.Lett.* **B596** (2004) 96, [hep-ph/0404004](#).
- [77] V. Cirigliano, G. Ecker, M. Eidemuller, R. Kaiser, A. Pich, *et al.*, *JHEP* **0504** (2005) 006, [hep-ph/0503108](#).
- [78] V. Cirigliano, G. Ecker, M. Eidemuller, R. Kaiser, A. Pich, *et al.*, *Nucl.Phys.* **B753** (2006) 139, [hep-ph/0603205](#).
- [79] K. Kampf and J. Novotny, *Phys.Rev.* **D84** (2011) 014036, [1104.3137](#).
- [80] J. Sanz-Cillero and A. Pich, *Eur.Phys.J.* **C27** (2003) 587, [hep-ph/0208199](#).
- [81] V. Mateu and J. Portolés, *Eur.Phys.J.* **C52** (2007) 325, [0706.1039](#).
- [82] A. Pich, [hep-ph/0205030](#).
- [83] G. Ecker, *Prog.Part.Nucl.Phys.* **35** (1995) 1, [hep-ph/9501357](#).
- [84] A. Pich, *Rept.Prog.Phys.* **58** (1995) 563, [hep-ph/9502366](#).
- [85] A. Pich, I. Rosell, and J. J. Sanz-Cillero, *JHEP* **1102** (2011) 109, [1011.5771](#).
- [86] I. Rosell, J. Sanz-Cillero, and A. Pich, *JHEP* **0408** (2004) 042, [hep-ph/0407240](#).
- [87] I. Rosell, J. J. Sanz-Cillero, and A. Pich, *JHEP* **0701** (2007) 039, [hep-ph/0610290](#).

- [88] J. Portolés, I. Rosell, and P. Ruiz-Femenía, *Phys.Rev.* **D75** (2007) 114011, hep-ph/0611375.
- [89] A. Pich, I. Rosell, and J. Sanz-Cillero, *JHEP* **0807** (2008) 014, 0803.1567.
- [90] J. Sanz-Cillero, *Phys.Lett.* **B681** (2009) 100–104, 0905.3676.
- [91] B. Moussallam, *Eur.Phys.J.* **C53** (2008) 401, 0710.0548.
- [92] J. Nieves, A. Pich, and E. Ruiz Arriola, *Phys.Rev.* **D84** (2011) 096002, 1107.3247.
- [93] A. Anisovich and H. Leutwyler, *Phys.Lett.* **B375** (1996) 335–342, hep-ph/9601237.
- [94] F. Niecknig, B. Kubis, and S. P. Schneider, *Eur.Phys.J.* **C72** (2012) 2014, 1203.2501.
- [95] K. Popper, *Conjectures and Refutations*. Routledge and Kegan Paul, London, UK, 1963. A. Pich, private communication, we are grateful to him for rising this point.
- [96] Belle Collaboration, D. Epifanov *et al.*, *Phys.Lett.* **B654** (2007) 65, 0706.2231.
- [97] W. Marciano and A. Sirlin, *Phys.Rev.Lett.* **61** (1988) 1815.
- [98] E. Braaten and C.-S. Li, *Phys.Rev.* **D42** (1990) 3888.
- [99] J. Erler, *Rev.Mex.Fis.* **50** (2004) 200, hep-ph/0211345.
- [100] S. Peris, M. Perrottet, and E. de Rafael, *JHEP* **9805** (1998) 011, hep-ph/9805442.
- [101] M. Knecht, S. Peris, M. Perrottet, and E. de Rafael, *Phys.Rev.Lett.* **83** (1999) 5230, hep-ph/9908283.
- [102] S. Peris, B. Phily, and E. de Rafael, *Phys.Rev.Lett.* **86** (2001) 14, hep-ph/0007338.
- [103] M. Golterman and S. Peris, *JHEP* **0101** (2001) 028, hep-ph/0101098.
- [104] M. Golterman, S. Peris, B. Phily, and E. De Rafael, *JHEP* **0201** (2002) 024, hep-ph/0112042.
- [105] P. Masjuan and S. Peris, *JHEP* **05** (2007) 040, 0704.1247.
- [106] P. Masjuan and S. Peris, *Phys. Lett.* **B663** (2008) 61, 0801.3558.
- [107] P. Masjuan, S. Peris, and J. J. Sanz-Cillero, *Phys. Rev.* **D78** (2008) 074028, 0807.4893.
- [108] O. Shekhovtsova, I. Nugent, T. Przedzinski, P. Roig, and Z. Was, 1208.5420.
- [109] P. Roig, I. Nugent, T. Przedzinski, O. Shekhovtsova, and Z. Was, 1208.4513.

- [110] Talks on Tau lepton conference, respectively by P. Roig, I. Nugent, O. Shekhovtsova, Z. Was, Nagoya Japan, September 2012, <http://tau2012.hepl.phys.nagoya-u.ac.jp/>.
- [111] P. Roig, *Nucl.Phys.Proc.Suppl.* **207-208** (2010) 145, 1010.0224.
- [112] <http://hibiscus.if.uj.edu.pl/~przedzinski/fifo.tgz>.
- [113] BaBar Collaboration Collaboration, B. Aubert *et al.*, *Phys.Rev.* **D77** (2008) 092002, 0710.4451.
- [114] J. Gómez Cadenas, A. Seiden, M. González-García, D. Coward, and R. Schindler, *Phys.Rev.* **D41** (1990) 2179.
- [115] J. Gómez-Cadenas, M. González-García, and A. Pich, *Phys.Rev.* **D42** (1990) 3093.
- [116] V. Cirigliano, G. Ecker, H. Neufeld, and A. Pich, *JHEP* **0306** (2003) 012, [hep-ph/0305311](http://hep-ph/0305311).
- [117] E. G. Floratos, S. Narison, and E. de Rafael, *Nucl.Phys.* **B155** (1979) 115.
- [118] G. Lepage and S. J. Brodsky, *Phys.Lett.* **B87** (1979) 359.
- [119] S. Weinberg, *Phys.Rev.Lett.* **18** (1967) 507.
- [120] Y.-H. Chen, Z.-H. Guo, and H.-Q. Zheng, 1201.2135.
- [121] P. Roig, *AIP Conf.Proc.* **964** (2007) 40, 0709.3734.
- [122] M. Dobbs and J. B. Hansen, *Comput. Phys. Commun.* **134** (2001) 41, <https://savannah.cern.ch/projects/hepmc/>.
- [123] R. Omnès, *Nuovo Cim.* **8** (1958) 316–326.
- [124] D. Boito, R. Escribano, and M. Jamin, *JHEP* **1009** (2010) 031, 1007.1858.
- [125] A. Pich and J. Portolés, *Phys.Rev.* **D63** (2001) 093005, [hep-ph/0101194](http://hep-ph/0101194).

## A Useful functions and notations

To minimize repetition and to reduce the size of formulas in Section 2 the lengthy ones were moved to this appendix.

In the description of the three-hadron currents the following functions were used:

$$\begin{aligned}
A^{\text{R}}(q^2, x, y, m_1^2, m_2^2, m_3^2) &= 3x + m_1^2 - m_3^2 + \left(1 - \frac{2G_V}{F_V}\right) [2q^2 - 2x - y + m_3^2 - m_2^2], \\
B^{\text{R}}(x, y, m_1^2, m_2^2) &= 2(m_2^2 - m_1^2) + \left(1 - \frac{2G_V}{F_V}\right) [y - x + m_1^2 - m_2^2], \\
A^{\text{RR}}(q^2, x, y, m_1^2, m_2^2, m_3^2) &= (\lambda' + \lambda'') (-3x + m_3^2 - m_1^2) \\
&\quad + (2q^2 + x - y + m_1^2 - m_2^2) H\left(\frac{x}{q^2}, \frac{m_2^2}{q^2}\right), \\
B^{\text{RR}}(q^2, x, y, z, m_1^2, m_2^2, m_3^2) &= 2(\lambda' + \lambda'') (m_1^2 - m_2^2) + (y - x + m_2^2 - m_1^2) H\left(\frac{z}{q^2}, \frac{m_3^2}{q^2}\right), \\
C^{\text{R}}(q^2, x, m_1^2, m_2^2, m_3^2) &= (c_1 - c_2 + c_5) q^2 - (c_1 - c_2 - c_5 + 2c_6) x \\
&\quad + (c_1 + c_2 + 8c_3 - c_5) m_3^2 + 8c_4 (m_1^2 - m_2^2), \\
C^{\text{RR}}(q^2, x, m^2) &= d_3 (q^2 + x) + (d_1 + 8d_2 - d_3) m^2, \\
D^{\text{R}}(q^2, x, y) &= (g_1 + 2g_2 - g_3) (x + y) - 2g_2 (q^2 + m_K^2) \\
&\quad - (g_1 - g_3) (3m_K^2 + m_\pi^2) + 2g_4 (m_K^2 + m_\pi^2) + 2g_5 m_K^2, \\
E^{\text{R}}(x, y) &= (g_1 + 2g_2 - g_3) (x - y). \tag{44}
\end{aligned}$$

They follow conventions of [25]. Function  $H(x, y)$  is defined in subsection 2.1, formula (7). In the description of the two pseudoscalar form factors, following [19, 20], the function  $A_{PQ}(s)$  was used to describe loops involving pions, kaons and  $\eta$  mesons

$$A_{PQ}(s) = -\frac{192\pi^2[sM_{PQ}(s) - L_{PQ}(s)]}{s}, \tag{45}$$

where

$$M_{PQ}(s) = \frac{1}{12s}(s - 2\Sigma_{PQ})\bar{J}_{PQ}(s) + \frac{\Delta_{PQ}^2}{3s^2}\tilde{J}_{PQ}(s) - \frac{1}{6}k_{PQ} + \frac{1}{288\pi^2}, \tag{46}$$

$$\Sigma_{PQ} = m_P^2 + m_Q^2, \quad \Delta_{PQ} = m_P^2 - m_Q^2, \quad k_{PQ} = \frac{F^2}{\Delta_{PQ}}(\mu_P - \mu_Q) \tag{47}$$

and

$$L_{PQ}(s) = \frac{\Delta_{PQ}^2(s)}{4s}\bar{J}_{PQ}(s). \tag{48}$$

The  $\mu_P = \frac{m_P^2}{32\pi^2 F^2} \ln\left(\frac{m_P^2}{\mu^2}\right)$  (at present we take  $\mu = M_\rho$  for all 2 pseudo-scalars modes<sup>42</sup>).

Finally,

$$\begin{aligned}\bar{J}_{PQ}(s) &= \frac{1}{32\pi^2} \left[ 2 + \left( \frac{\Delta_{PQ}}{s} - \frac{\Sigma_{PQ}(s)}{\Delta_{PQ}} \right) \ln \frac{m_Q^2}{m_P^2} - \frac{\nu}{s} \ln \frac{(s+\nu)^2 - \Delta_{PQ}^2}{(s-\nu)^2 - \Delta_{PQ}^2} \right], \\ \tilde{J}_{PQ}(s) &= \bar{J}_{PQ}(s) - s\bar{J}'(0),\end{aligned}\tag{49}$$

where  $\nu^2 = \lambda(s, m_P^2, m_Q^2)$ . Care has to be taken to keep the imaginary part of  $\nu^2$  in the phase-space regions where  $\nu^2 < 0$ , and where  $Im \nu$  must not be set to zero, see the function JPQ1\_FUNCT in the file `funct_rpt.f`. In the vector form factor for two pions, this effect shows up in the  $KK$  contribution to the loop function from below the threshold of  $KK$  production.

For the  $\rho'$  and  $\rho''$  mesons the loop function  $A_\pi(s)$  taken from [51] reads:

$$A_\pi(s) = \ln\left(\frac{m_\pi^2}{\mu^2}\right) + 8\frac{m_\pi^2}{s} - \frac{5}{3} + \sigma_\pi^3 \ln\left(\frac{\sigma_\pi + 1}{\sigma_\pi - 1}\right).\tag{50}$$

In the last formulas the  $SU(2)$  limit is taken and  $m_{\pi^\pm} = m_{\pi^0} = 0.13804$  GeV.

All functions in this appendix are coded in file `new-currents/RChL-currents/funct_rpt.f`.

## B Installation

Our project tar-ball, even though resulting from a rather large effort, is not designed for independent installation. This would be of course straightforward and we will return to that solution in the future, once the currents are optimized to improve agreement with the data. The parametrization will become integrated part of the TAUOLA distribution; for fortran or for C++ use, like in references [14, 62]. At present we concentrate on a solution which is most convenient for the experimental user e.g. from Belle or BaBar collaboration aiming at combining the code with the version of TAUOLA which is already being used as part of the simulation set-up. We aim at preparing an add-up<sup>43</sup> for already existing set-up. The tar-ball can be downloaded from the Web page [28] of our project.

Once tar-ball is unpacked inside TAUOLA-FORTRAN/tauola subdirectory (of user environment), the directory `tauola/new-currents` will be created, all necessary fortran files will be found there. For convenience, later on, we will use the following aliases:

- `#{RCHLCURRENTS}` instead of `tauola/new-currents/RChL-currents`.
- `#{OTHERCURRENTS}` instead of `tauola/new-currents/other-currents`.
- `#{INSTALLATION}` instead of `tauola/new-currents/Installation`.

<sup>42</sup>Alternatively, for  $\mu$  we may take  $M_\rho$  for  $PQ = \pi\pi$ ,  $KK$  and  $M_{K^*}$  for  $PQ = K\pi$  [29].

<sup>43</sup>As the project is developed under svn, the tar-ball is accompanied with svn label and it should be kept for reference.

In `tauola/new-currents` further sub-directories for more advanced use or for documentation will be found:

- `#{RCHLCURRENTS}/tabler/a1` - programs for pretabulations in particular of  $q^2$ -dependent  $a_1$  width<sup>44</sup>.
- `#{RCHLCURRENTS}/cross-check` - code for technical and numerical tests.
- `new-currents/paper` - present paper.
- `#{INSTALLATION}` - instructions for modifications to be introduced in FORTRAN files and makefile residing in directory `tauola`.
- `new-currents/Installation-Reweight` - instruction and example of using reweighting algorithm.

None of the directories listed above contains code which is to be loaded together with TAUOLA library. Code loaded with the library is located only in the main folder of `#{RCHLCURRENTS}` and `tauola/new-currents/other-currents`. Programs in `#{RCHLCURRENTS}/tabler/a1` can update the fortran code located in file `#{RCHLCURRENTS}/initA1Tab.f`.

Once installation is completed, to invoke the calculation of our new currents the `CALL INIRChL(1)` has to be invoked<sup>45</sup> by user main program prior to call on TAUOLA initialization. If instead `CALL INIRChL(0)` is executed prior<sup>46</sup> initialization, old currents - as in Ref. [14] - will be used in generation.

The `CALL INIRChL(1)` may activate also new currents<sup>47</sup> e.g. for  $\eta\pi\pi$  or  $4\pi$  decay channels. At present only wrappers of currents of Ref. [14] and [33] are prepared in the directory `#{OTHERCURRENTS}` for convenience of users and our future work. These currents lead to substantially different distributions, that is why, one may require adjustment of phase space presampler used to optimize speed of generation. Anyway, as a default, they are turned off. For `INIRChL(1)` the same TAUOLA `cleo` currents as for `INIRChL(1)` are used. To turn other options, `ISWITCH` located in the file `#{OTHERCURRENTS}/ffourpi.f` has to be changed from its default value 0 to 1, 2, 3 or 4.

## B.1 Changes for host TAUOLA version

In order to use new currents, changes have to be made to the host TAUOLA installation. Let us document here in great detail changes to be introduced in TAUOLA `cleo` version. If

---

<sup>44</sup>In the directory `#{RCHLCURRENTS}/tabler` the place to calculate other pretabulated functions (as possibly the scalar form factor for  $K\pi$  channel) is reserved.

<sup>45</sup>For a C++ user, examples of use of `inirchl_(1)` are given in `new-currents/Installation-Reweight/` directory.

<sup>46</sup>This can be done also after initialization as no initialization of tables is needed. Then one can revert the change again with `CALL INIRChL(0)`.

<sup>47</sup>Although the  $\tau \rightarrow \eta^{(\prime)}\pi^-\pi^0\nu_\tau$  decays have been worked out within Resonance Chiral Theory [111], the corresponding expressions for the currents have not been incorporated yet to the program.

some modifications were introduced and user's host TAUOLA installation differs from TAUOLA cleo of Ref. [14], then modifications prepared in  $\{\text{INSTALLATION}\}$  directory can not be used directly and some adaptation may be necessary. In either case we advice to check if at least some of the numerical results from Ref. [28] are correctly reproduced after installation.

Let us list now changes which have to be introduced to files residing in TAUOLA/tauola directory of the user installation .

- TAUOLA/tauola/makefile

The list of LIB\_OBJECTS must be extended and additional objects added:

```
 $\{\text{RCHLCURRENTS}\}/f3pi_rcht.o, \{\text{RCHLCURRENTS}\}/fkkpi.o,$ 
 $\{\text{RCHLCURRENTS}\}/fkk0pi0.o, \{\text{RCHLCURRENTS}\}/wid_a1_fit.o,$ 
 $\{\text{RCHLCURRENTS}\}/frho_pi.o, \{\text{RCHLCURRENTS}\}/funct_rpt.o,$ 
 $\{\text{RCHLCURRENTS}\}/value_parameter.o, \{\text{RCHLCURRENTS}\}/initA1Tab.o,$ 
 $\{\text{RCHLCURRENTS}\}/fkpi1.o, \{\text{RCHLCURRENTS}\}/fk0k.o,$ 
 $\{\text{OTHERCURRENTS}\}/fetapi.o, \{\text{OTHERCURRENTS}\}/ffourpi.o,$ 
 $\{\text{OTHERCURRENTS}\}/binp.o, \{\text{OTHERCURRENTS}\}/curr_karls.o,$ 
 $\{\text{OTHERCURRENTS}\}/curr_karls_extracted.o;$ 
```

if there are no additional dependencies the  $\{\text{INSTALLATION}\}/makefile-tauola$  file can be simply copied into tauola/makefile .

- TAUOLA/tauola/tauola.f

If the file in user's version coincides with the one of TAUOLA cleo distribution, the  $\{\text{INSTALLATION}\}/tauola.f-new$  file can be simply copied into tauola/tauola.f . To verify this, the diff file  $\{\text{INSTALLATION}\}/tauola.f-oldDIFFupdated$  may be inspected.

- TAUOLA/tauola/formf.f

If the file in user's version coincides with the one of TAUOLA cleo distribution, the  $\{\text{INSTALLATION}\}/formf.f-new$  file can be simply copied into tauola/formf.f . To verify this, the diff file  $\{\text{INSTALLATION}\}/formf.f-oldDIFFupdated$  may be inspected.

Once changes are introduced the new currents will be activated and the old ones will be overruled once call to routine INIRChL(1) is invoked. Otherwise, or if CALL INIRChL(0) is invoked (at any time), old currents will be then switched back on. The routine INIRChL(1) has to be invoked by the user program at the initialization step. For the C++ user, a definition of extern "C" void inirchl\_(int i); has to be included and execution of inirchl\_(&i); performed.

An example has been provided in  $\{\text{INSTALLATION}\}/demo-standalone$  . It is based on default TAUOLA cleo example with the only modification being the call to INIRChL(1) before default TAUOLA initialization.

## B.2 Calculating numerical tables used by form factors

The directory `#{RCHLCURRENTS}/tabler/a1` contains the program `dalwid_tot_rho1_gauss.f`; it creates a table of  $\Gamma_{a_1}(q^2)$  according to Eq. (35). The system does not use any information from TAUOLA initialization except the pion and kaon masses.

We have also prepared a place to add tables for other functions, in the near future it will be done for the scalar form factor of the  $K\pi$  mode.

### B.2.1 Executing the code

The program `dalwid_tot_rho1_gauss.f` produces the  $q^2$  distribution of the  $a_1$  off-shell width.

To compile, type `make` in `#{RCHLCURRENTS}/tabler/a1` directory. To run, type `make run`. Each line of the produced output includes the value of  $q^2[\text{GeV}^2]$ , and the value of  $d\Gamma/dq^2[\text{GeV}^{-1}]$ . This table is written into the file `initA1Tab.f` which is the FORTRAN code ready to use. One can shift it to `#{RCHLCURRENTS}` directory by `make move` command. Text format table is written into file `wida1_qq_tot_2e5.out`.

### B.2.2 Setup

Input parameters and common blocks are located in `#{RCHLCURRENTS}/parameter.inc`. Other parameters are defined in `#{RCHLCURRENTS}/value_parameter.f`. These parameters may be changed by the user. If the parameters affect the  $q^2$ -dependent  $a_1$  width (or other pretabulated functions), the tables need to be generated anew with the help of programs residing in the directory `#{RCHLCURRENTS}/tabler`. A list of the parameters that affect generated tables (and thus require tables to be generated again) is in `#{RCHLCURRENTS}/value_parameter.f`. Some of the variables used in functions from `#{RCHLCURRENTS}/funct_rpt.f` are declared in `#{RCHLCURRENTS}/funct_declar.inc`.

## B.3 Tests

Directory `#{RCHLCURRENTS}/cross-check` contains three subdirectories:

1. `check_analyticity_and_numer_integr`, it includes:
  - test of numerical stability in calculations of  $\Gamma_{a_1}(q^2)$  and for the whole  $\tau$  hadronic decays as described in Section 2. For that purpose it is checked if continuity of results as a function of the invariant mass holds.
  - the result for the integrated width of the  $\tau \rightarrow 2\pi\nu_\tau$ ,  $\tau \rightarrow K\pi\nu_\tau$ ,  $\tau \rightarrow K^-K^0\nu_\tau$ ,  $\tau \rightarrow 3\pi\nu_\tau$ ,  $\tau \rightarrow K\pi^-K\nu_\tau$  and  $\tau \rightarrow K^-\pi^0K^0\nu_\tau$ . These results can be confronted with the result of Monte Carlo simulation collected in sub-directory `tauola_result_modes`.



2. `results_numer_integr_3pion` presents the results for the width of  $\tau \rightarrow 3\pi\nu_\tau$  as a function of the 3 pion invariant mass. It is calculated by numerical integration of the analytical formula for different choices of hadronic form factors as it is described in Section 4.
3. `tauola_result_modes` contains Monte Carlo results for both differential and total width for the processes  $\tau \rightarrow 2\pi\nu_\tau$ ,  $\tau \rightarrow K\pi\nu_\tau$ ,  $\tau \rightarrow K^-K^0\nu_\tau$ ,  $\tau \rightarrow 3\pi\nu_\tau$ ,  $\tau \rightarrow K\pi^-K\nu_\tau$  and  $\tau \rightarrow K^-\pi^0K^0\nu_\tau$ .

### B.3.1 Numerical stability tests

The directory `/${RCHLCURRENTS}/cross-check/check_analyticity_and_numer_integr` contains six subdirectories with tests of numerical stability for hadronic  $\tau$  decay modes and a subdirectory with the test for the  $a_1$  width. Each decay channel is located in a separate directory. Details regarding each of these tests are described in `README` files of the directory and every subdirectory as well. That is why only the basic information is provided in our paper. We have checked using interpolation from neighbouring values that the value of  $d\Gamma/dq^2$  is continuous and is not contaminated by numerical instability of multidimensional Gaussian integration. Also we present the analytical results for the partial width of every channel to be compared with the Monte Carlo ones.

Content of the directory:

- `check_analyt_3piwidth`: test of numerical stability of the distribution  $d\Gamma(\tau \rightarrow \nu_\tau\pi\pi\pi)/dq^2$ . Results are presented for separate modes:  $d\Gamma(\tau \rightarrow \nu_\tau\pi^0\pi^0\pi^-)/dq^2$  and  $d\Gamma(\tau \rightarrow \nu_\tau\pi^-\pi^-\pi^+)/dq^2$ . Also the value of the partial widths for the channels is provided for the comparison with the TAUOLA results.
- `check_analyt_kkpi` - test of numerical stability for  $d\Gamma(\tau \rightarrow \nu_\tau KK\pi)/dq^2$ . Results are presented for separate modes:  $d\Gamma(\tau \rightarrow \nu_\tau K^-\pi^-K^+)/dq^2$  and  $d\Gamma(\tau \rightarrow \nu_\tau K^0\pi^-K^0)/dq^2$ . The value of the partial widths for both channels are provided.
- `check_analyt_kk0pi0` - tests of numerical stability for  $\tau \rightarrow \nu_\tau K^-\pi^0K^0$ : both the spectrum  $d\Gamma(\tau \rightarrow \nu_\tau K^-\pi^0K^0)/dq^2$  and the partial width are provided.
- `check_analyt_2pi` - tests of numerical stability for  $\tau \rightarrow \nu_\tau\pi^-\pi^0$ : both the spectrum  $d\Gamma(\tau \rightarrow \nu_\tau\pi^-\pi^0)/dq^2$  and the partial width are provided.
- `check_analyt_kpi` - tests of numerical stability for  $\tau \rightarrow \nu_\tau K\pi$ : both the spectrum for the total width  $d\Gamma(\tau \rightarrow \nu_\tau K\pi)/dq^2$  and the partial width for channels  $\pi^-K^0$  and  $\pi^0K^-$  are provided. The partial widths for the individual decays are checked to be 2/3 and 1/3 of the total  $K\pi$  width, mass effects are negligible in this case.
- `check_analyt_k0k` - tests of numerical stability for  $\tau \rightarrow \nu_\tau K^-K^0$  both the differential distribution  $d\Gamma(\tau \rightarrow \nu_\tau K^-K^0)/dq^2$  and the partial width are provided.
- `check_analyt_a1table` - tests of numerical stability of  $\Gamma_{a_1}(q^2)$  produced by program described in Appendix B.2.

### B.3.2 Analytic integration test

The results of the analytical integration test in the three-pion case are presented in the directory `/${RCHLCURRENTS}/cross-check/results_numer_integr_3pion`. They are produced by the program `totwid3pi_qq_table.f` in the directory `/${RCHLCURRENTS}/cross-check/check_analyticity_and_numer_integr/check_analyt_3pi`. The program can be compiled by command `make` and run with `make totwid3pi_run > output.txt`.

The setup file `input_f1f2f4.dat`, in `/${RCHLCURRENTS}/cross-check/check_analyticity_and_numer_integr/check_analyt_3pi` contains:

- `eps` - defines (relative) precision of the Gaussian integration.
- `kf1` - flag for form factor  $F_1$ . For `kf1= 0, 1` or `2`  $F_1$  will be set respectively to 0, 1 or to its functional form.
- `kf2` - flag for form factor  $F_2$ . For `kf2= 0, 1` or `2`  $F_2$  will be set respectively to 0, 1 or to its functional form.
- `kf4` - flag for form factor  $F_4$ . For `kf4= 0, 1` or `2`  $F_4$  will be set respectively to 0, 1 or to its functional form.
- `chan` - flag to choose the 3 pion mode. `chan= 1` for  $\pi^0\pi^0\pi^-$  and `chan= 2` for  $\pi^-\pi^-\pi^+$ .

If the functional form of the form factors is used, it will be taken from the file `/${RCHLCURRENTS}/cross-check/check_analyticity/check_analyt_3piwidth/funct_3pi.f`. If `kf1` or `kf2` is set to 2, pretabulated file `/${RCHLCURRENTS}/initA1Tab.f` will be used for  $\Gamma_{a_1}$  in the propagator of the  $a_1$ -meson<sup>48</sup>.

Output file contains four columns:

- `qmin` (in  $[\text{GeV}^2]$ ) - lower boundary for the integration over 3-pion invariant mass.
- `qmax` (in  $[\text{GeV}^2]$ ) - upper boundary for the integration over 3-pion invariant mass.
- `eps` - estimate of the integration precision in the result.
- total width (in  $[\text{GeV}]$ ).

Results for the different configurations of the form factor are presented in `tauola/RChL-currents/cross-check/results_numer_integr_3pion`.

---

<sup>48</sup>Note that the tabulated file is generated by the program described in Appendix B.2.

## B.4 TAUOLA weight recalculation mode

Let us present now the installation necessary for the method of weighted events, which was envisaged in Section 6.1. An example of such installation code is included in our distribution tar-ball in directory `new-currents/Installation-Reweight`.

Before reweighting method can be used, TAUOLA needs to be adapted to new currents as explained in the Appendix B.1. Afterwards, our example program `tau-reweight-test-ASCII.c`, residing in the directory `new-currents/Installation-Reweight`, can be run with the help of the simple `make` command<sup>49</sup>. For more details regarding the reweighting examples, refer to `README` located in `new-currents/Installation-Reweight`.

The following subsection describes reweighting algorithm as well as initialization used in the example. Note, contrary to the rest of the project, reweighting algorithm, including examples of its usage, is written in C++.

### B.4.1 Weight recalculation algorithm

In order to use recalculation mode, several steps have to be performed from user program:

1. Before TAUOLA initialization, RChL currents have to be switched on. This can be done with the help of the wrapper for FORTRAN function `INIRChL(IVER)`, by calling `inirchl_(&i)`; with `i = 1`; . Two versions of currents will be used, but initialization must be done for `IVER=1`, for initialization of RChL-specific variables and tables.
2. Initialization of TAUOLA must be called. We are using initialization taken from the default TAUOLA example, stored in wrapper function `f_interface.tauolaInitialize`.
3. For each event, the information about  $\tau$  and its decay products must be filled and stored in instances of `SimpleParticle` class<sup>50</sup>.
4. Once the kinematical configuration for  $\tau$  decay is read from the datafile (or fifo pipe), function: `double calculateWeight(SimpleParticle &tau, vector<SimpleParticle> &tau_daughters)` can be used to retrieve the weight.

The algorithm of the function `calculateWeight` is sketched in the following:

1. Particles are prepared and boosted to the appropriate frame.
2. TAUOLA decay channel is identified.

---

<sup>49</sup>Other example, `tau-reweight-test-HepMC.c`, requires installation of `HepMC` and optional installation of `MC-TESTER`, and their paths provided in the `Makefile`.

<sup>50</sup>Class `SimpleParticle` is used only to contain four-vector and flavour of the particle.

3. TAUOLA cleo currents are switched on with `inirchl_(&i); i = 0.`
4. Call to appropriate internal TAUOLA FORTRAN subroutine, returning weight WT1.
5. RChL currents are switched on with `inirchl_(&i); i = 1.`
6. Call to the same routine as in step 4 is performed, returning weight WT2.
7. Ratio of weights calculated at steps 4 and 6 gives required model replacing weight.
8.  $WT = WT2/WT1$  is returned to the main user program.

It is rather straightforward to extend this method to the case when more than one new version of physics initialization is to be used. Note that the examples are set up so that the weight is calculated both for  $\tau^-$  and  $\tau^+$  and stored in variables WT\_M and WT\_P respectively. In cases where only a single  $\tau$  is present in the event, the weight corresponding to the second  $\tau$  equals 1.0.

Alternatively, in cases when this approach cannot be used or is inconvenient, variants of the method, based on fifo pipes can be useful as well. Prototypes for such solutions can be obtained from Ref. [112].

Hadronic currents for  $\tau^+$  and  $\tau^-$  differ due to CP parity. The resulting effects are taken into account in the reweight algorithm.

## B.5 TAUOLA++ installation

Thanks to the modular construction of TAUOLA C++ Interface [62], new currents can be used in C++ projects in a straightforward way. It is enough to replace the previous TAUOLA-FORTRAN installation with the new one, adjusting Makefile with a list of the newly added object files.

For step-by-step instructions, we refer to `INSTALLATION/README-TAUOLA++`. Our package has already been tested to work with TAUOLA C++ Interface v1.0.5, but the installation procedure is similar for all previous versions and should remain unchanged for future versions as well.

## C Input parameters

The results collected in this paper represent a technical test of program installation as well. Figures should be reproduced if the input parameters, collected in Tables 3, 4, and 5 and defined in routine `tauola/new-currents/RChL-currents/value_parameter.f` remain unmodified. In some cases the actual numerical value of parameters depends on chosen decay channel. For the  $KK\pi$  modes we use  $M_{K^*} = (M_{K^{*\pm}} + M_{K^{*0}})/2$ . For the  $K\pi$  modes the value of parameters depends on parametrization. It is distinct for the one of Ref. [27] and of Ref. [50]. In the second case the mass parameters are noticeably different from the pole values. The results for the latter are consistent in both approaches.

The choice between the two parametrizations for  $K\pi$  modes (channels 2, 3 in Table 6) is controlled by `FFKPIVEC` again to be set in `value_parameter.f`. The `FFKPIVEC = 0` activates parametrization from Ref. [50] and `FFKPIVEC = 1` the ones of [27]. Numerical values of all parameters, not only the masses, are different for the two cases. Variables are named with big greek letters for `FFKPIVEC = 1` and with the small ones for `FFKPIVEC = 0`.

There are two other flags `FFVEC` and `FFKKVEC` in `value_parameter.f`. The first one fixes run with/without FSI effects (`FFVEC = 1` for run with FSI effects) and the last one chooses the parametrization for two-kaon form factor with/without the excited  $\rho$  meson states (`FFKKVEC = 1` for the parametrization with  $\rho'$  and  $\rho''$ ). By default `FFVEC = 1`, `FFKPIVEC = 1` and `FFKKVEC = 0`.

On technical side, the choice of the internal flag `KAK` is made at the start of each  $\tau$  decay generation. It depends on the decay channel labelled by `imode` (generated by `TAUOLA`) and the flags<sup>51</sup> `FFVEC`, `FFKKVEC` and `FFKPIVEC`. The variable `KAK` is then passed into routine `value_parameter.f` and the appropriate choice for the parameters is made. The `KAK` parameter coincides with `imode` for all channels except the  $K\pi$  modes. For the  $K\pi$  decay modes `KAK = 70` if `FFKPIVEC = 0` and `KAK = 71` if `FFKPIVEC = 1`.

For `FFKPIVEC = 0` (that is for `KAK = 70`) parameters marked in Tables with † are used, otherwise defaults of Tables 4 and 5 are left unmodified.

For `KAK=4` (i.e., for  $\tau \rightarrow \pi^- \pi^0 \nu_\tau$ ) masses and widths of  $\rho, \rho'$  and  $\rho''$  result from the adjustment to the experimental data and do not coincide with PDG defaults. For other channels we simply take the PDG values [31] for the  $\rho(\rho')$  parameters. The PDG values are also taken for the narrow width resonances  $\omega$  and  $\phi$ , numerical values are collected in Table 3.

The PDG value is taken for the  $a_1$  mass<sup>52</sup>. The parameters of the Resonance Chiral Theory are given in the Table 4 as well<sup>53</sup>.

The parameters  $\theta_V$  and  $F_K$  can be varied by the user starting from the code version of the year 2012. We follow Ref. [25] and the case of ideal mixing ( $\theta_V = 35.26^\circ$ ). In this case the  $\phi$  contribution to  $\tau \rightarrow KK\pi\nu_\tau$  vanishes [25]. However, the absence of intermediate  $\phi$  exchange contradicts the results of the BaBar Collaboration [113] for the isospin related decay  $e^+e^- \rightarrow K^+\pi^0K^-$  and for  $\tau$  decays themselves (see<sup>10</sup>). The parameter  $F_K$  is not used in our default formulas. It enters the non-default parametrization for  $K\pi$  vector form factor, i.e., for `FFKPIVEC = 0`, `KAK = 70`. We follow Ref. [50] in the choice  $F_K = 1.198 \cdot F$ .  $F_K \neq F$  is related to  $SU(3)$  breaking and higher-order chiral corrections. The parameter  $H_{t0} = -1.24004 \cdot 10^{-2}$  does not appear in the text either. It corresponds to the value of the  $K\pi$  loop function at zero-momentum transfer,  $\tilde{H}_{K\pi}(0)$ , in Eq.(11) of

<sup>51</sup>At the moment `KAK` depends on `FFKPIVEC` only. However, in future it will depend also on `FFVEC` and `FFKVEC`.

<sup>52</sup>For discussion on the difference between the mass used in the resonance Lagrangian and the physical one and a possibility to substitute the first with the latter, see [25] and footnote<sup>56</sup> in this paper.

<sup>53</sup>We point out that the values for the parameters  $\Gamma_{\rho'}$ ,  $M_{\rho''}$ ,  $\Gamma_{\rho''}$ ,  $\gamma$ ,  $\delta$ ,  $\phi_1$  and  $\phi_2$  lie outside the educated guess for its range of variation given in Table 4. This is irrelevant for the technical check we are proposing in this Section but matters for the actual use of the program.

Ref. [50].

Parameter	Var. name	Default	Used in channel
$m_\tau$	MTAU	1.777	all,*
$m_{\nu_\tau}$	MNUTA	0.001	all,*
$\cos\theta_{\text{Cabibbo}}$	set in TAUOLA init.	0.975	all
$G_F$	set in TAUOLA init.	$1.166375 \cdot 10^{-5}$	all
$m_{\pi^\pm}$	mpic	0.13957018	all,*
$m_{\pi^0}$	mpiz	0.1349766	all,*
$m_\eta$	meta	0.547	2,3,5-9,*
$m_{K^\pm}$	mkc	0.493677	all,*
$m_{K^0}$	mkz	0.497648	all,*
$M_\omega$	mom	0.78194	7,8
$\Gamma_\omega$	gom	0.00843	7,8
$M_\phi$	mphi	1.019	7,8
$\Gamma_\phi$	gphi	0.0042	7,8

Table 3: Initialization parameters defined in TAUOLA main code or in file `new-currents/RChL-currents/value_parameter.f`: constants and defaults. In this table our defaults used for plots or parameters not requiring to be changed in fits are collected. Channels identification numbers are defined in Table 6. Energy units are powers of GeV. Variables requiring rerun of pretabulation `new-currents/RChL-currents/tabler/a1/dalwid_tot_rho1_gauss.f` are marked with \*.

Let us stress that in practice the parameters may need to be varied. The defaults and the expected variation ranges are given in Tables 4 and 5.

## C.1 Range of variation of the non-resonance input parameters

As long as the PDG values do not change, the values listed in Table 3 should remain unchanged<sup>54</sup>.

In order to account for the uncertainty given by higher-order chiral corrections, we suggest to vary  $F_K$  as indicated in Table 4.

## C.2 Range of variation of the resonance input parameters

The resonance parameters are of different nature in this respect. Apart from the safe identification  $M_V \equiv M_\rho$  [116], there is more uncertainty and model dependence on them. For the program user this is translated in a relative freedom to change the values of  $M_\rho$ ,

<sup>54</sup>The PDG limit on  $m_{\nu_\tau}$  (18.2 MeV) is not used in the program. If one wants to play with this limit [114, 115], our test results shall change in a rather negligible way. We use  $m_{\nu_\tau} = 0.01$  GeV.

$M_{a_1}, M_{\rho'}, \Gamma_{\rho'}, M_{\rho''}, \Gamma_{\rho''}, \gamma, \delta, \phi_1, \phi_2, M_{K^{*\pm}}, M_{K^{*0}}, M_{K^*}, M_{K^{*'}}, m_{K^*}, m_{K^{*'}}, \gamma_{K^*}, \gamma_{K^{*'}}$ ,  $\Gamma_{K^{*'}}$ ,  $F_V, G_V = F^2/F_V$  (although some deviations to this relation -below 20%- may be expected due to the effect of excited resonances),  $F_A, \beta_\rho$  and  $\gamma_{K\pi}$ . The changes of these parameters can be guided by the educated guesses on their range<sup>55</sup>, displayed in Table 4.

The warning is that the  $F_V$  and  $F_A$  cannot be changed independently since they should satisfy, to a reasonable accuracy<sup>56</sup>, the first and second Weinberg sum rules taken in the single resonance approximation [119]:

$$F_V^2 - F_A^2 = F^2, \quad F_V^2 M_V^2 = F_A^2 M_A^2. \quad (51)$$

Violations of these relations can be due to the modelization of the resonance spectrum in the large- $N_C$  limit but should remain below 20%.

There is more uncertainty on the couplings belonging to the odd-intrinsic parity sector, namely the  $c_i, d_i$  and  $g_i$  values and variation ranges are given in Table 5. Some remarks on the relations are in place:

- $c_1 - c_2 + c_5 \neq 0$  would violate maximally the short-distance QCD-ruled behaviour for the vector-vector correlator  $\Pi_V(q^2)$  [25], this condition must not be changed.
- $2g_4 + g_5$  comes from  $\Gamma(\omega \rightarrow \pi^+\pi^-\pi^0)$ . Both the direct production mechanism [25] and the one-resonance exchange [46] were taken into account consistently and the error is under control:  $2g_4 + g_5 = -0.60 \pm 0.02$ . If the PDG value for this decay width does not change, the value of this combination of couplings should be changed within the quoted error only.
- The high-energy large- $N_C$  predictions for the set  $\{g_2, g_1 - g_3, c_1 - c_2 - c_5 + 2c_6, d_3\}$  come at the same order in the expansion of  $\Pi_V(q^2)$  in powers of  $1/q^2$  [25]. Therefore, changes on the values of these parameters shall be expected from subleading corrections in  $1/N_C$  and, moreover, they will be highly correlated. Variations of 1/3 with respect to the values of any of them, see Table 5, may occur.
- The predictions for  $d_1 + 8d_2 - d_3$  and  $c_1 + c_2 - 8c_3 - c_5$  were not obtained in hadronic  $\tau$  decays but in the study of the  $\langle VVP \rangle$  octet [46] and singlet [120] Green function. Therefore, an educated conservative guess yields a deviation up to some 50% of the former. For the latter, a non-zero value may arise provided it has a minor effect in the observables, since its contribution vanishes in the chiral limit.

---

<sup>55</sup>Keep in mind, however, the warning concerning the relation  $G_V = F^2/F_V$  and the one affecting Eq.(51) for the range for  $G_V$  and  $F_A$ , respectively.

<sup>56</sup>Checking the first of Eqs. (51) is straightforward; for the second one, it should be observed that in the different relations among couplings which can be obtained from short-distance QCD constraints [67, 68, 117, 118] and involving  $M_A$ , the identification  $M_A \sim M_{a_1}$  is not appropriate [116]. There is some tension on the value of  $M_A$ : 998(49) MeV in Ref. [81] versus 920(20) MeV in Ref. [85]. The range [900, 1050] MeV should accommodate reasonable variations of this parameter in order to estimate the possible violations of the second Weinberg sum rule. The interval given for  $M_{a_1}$  is only marginally consistent with the PDG value [31]. However, this is not an issue, since it depends strongly on the precise definition of the resonance mass used to extract it; the PDG one and the one in Ref. [24] are different.

- Our current understanding seems to point to different values of  $c_4$  and  $g_4$  than those shown in Table 5. We would suggest that they are allowed to vary freely in the fits (keeping control on the branching ratio if it is not included as a data point in the fit).

In addition to what is explained above, the values of the couplings can be affected by the introduction of the second multiplet of resonances in  $\tau \rightarrow KK\pi\nu_\tau$  decays.

Finally there are parameters in `value_parameter.f` which are already prepared for the future update, but not yet used in the program: `gro`, `mf2`, `gf2`, `mf0`, `gf0`, `msg`, `gsg`.

## D Benchmark results

In Table 6 we collect results as coming from our default setting. It documents directly the distribution tar-ball. Results have to be checked once tar-ball is unpacked and installed in the particular environment. It will check if sufficiently large samples are installed, correctness of coupling constant setting, etc. This table will be updated in the future, once currents are modified, and included in the paper; version of the distribution tar-ball.

A wealth of data is available from the project Web page [28]. Many of the results collected there were obtained using MC-TESTER [57]. The distributions can be thus easily used for benchmarking any other Monte Carlo program independently if it is used for simulations coded in C++ or FORTRAN, provided that event record such as HEPEVT or HepMC [122] is used.

## E Final state interactions

Final state interactions have been taken into account for the two-meson  $\tau$  decays but not for the three-meson channels. It is of great importance to include them in the two-meson decays, because otherwise the right normalization at the peak is clearly lost and the curve would go systematically below the data in the resonance region<sup>57</sup>. This effect is certainly much smaller for the three-meson  $\tau$  decays, where nonetheless it can show up in the two-particle invariant mass distributions in particular regions of phase space, where our calculation is particularly far from experimental data, see Fig. 8. For the two-meson modes ( $\tau \rightarrow PQ\nu_\tau$ ), FSI are taken into account through the Omnès resummation [123] provided by the exponents in Eqs. (24) and (27). In this approximation [51], the imaginary part of the loop function is kept in the denominator, providing the width of the exchanged resonance. The real part is resummed in the exponential –while the exponential is a common factor in Eq. (27), it is different in every term in Eq. (24). If we had good theoretical knowledge of the energy-dependent meson widths (also for excited resonances) the latter procedure would be preferable. For the time being, both approaches are equivalent within the theoretical

---

<sup>57</sup>This reduction of the  $|F_V^{PQ}(s)|^2$  peak value amounts to 13%  $\leftrightarrow$  30% for  $PQ = \pi\pi$ ,  $KK$ , and  $K\pi$ , depending on the decay channel and the exchanged resonances accounted for. See also the analogue comparison for the decay width in Section 5.4.



uncertainties. This resummation respects analyticity and unitarity only in a perturbative sense, a feature that can be improved [50] to hold to all orders as follows:

1. The relevant phase-shift is obtained as the ratio between the imaginary and real parts of the vector form factor  $\delta^{PQ}(s) = Im [F_V^{PQ}(s)] / Re [F_V^{PQ}(s)]$ .  $F_V^{PQ}(s)$  stands for a form factor which can be obtained from Eqs. (24), (26) and (27) by taking out the exponentials and placing back the real part of the relevant loop functions in the denominator (see Refs. [29] and [52] for details).
2. A three-times subtracted dispersion relation is used to resum FSI effects and the final form factor reads

$$F_V^{PQ}(s) = \exp \left\{ \alpha_1 s + \alpha_2 s^2 + \frac{s^3}{\pi} \int_{s_{thr}}^{s_{cut}} ds' \frac{\delta^{PQ}(s')}{s'^3(s' - s - i\epsilon)} \right\}, \quad (52)$$

with  $s_{cut} \sim 4 \text{ GeV}^2$  [50, 124, 125] and  $s_{thr} = (m_P + m_Q)^2$ . The subtraction constants  $\alpha_1$  and  $\alpha_2$  are to be fitted to data.

This procedure will be followed in a future update of the program. Technically the method requires calculation of Cauchy Principal Value integrations which can be rather time-consuming and necessitates numerical stability checks.

For the moment we consider FSI effects as they are given in Chapter 2.4, Eqs. (23)-(27). To run the code with the FSI effects one has to fix `FFVEC = 1` in `value_parameter.f`. Effects of FSI are presented in Table 6, last four lines are provided for comparison, and in Fig. 10, they change by 14% – 32% the decay width, depending on the channel. Further results are collected in our Web page [28].

In the three-meson modes these interactions are neglected at the moment. We plan to include them in the future, at least for the  $\tau \rightarrow \pi\pi\pi\nu_\tau$  decays.

Comparison of Mass(1) of K- pi0 in channel tau- => K- pi0 nu\_tau

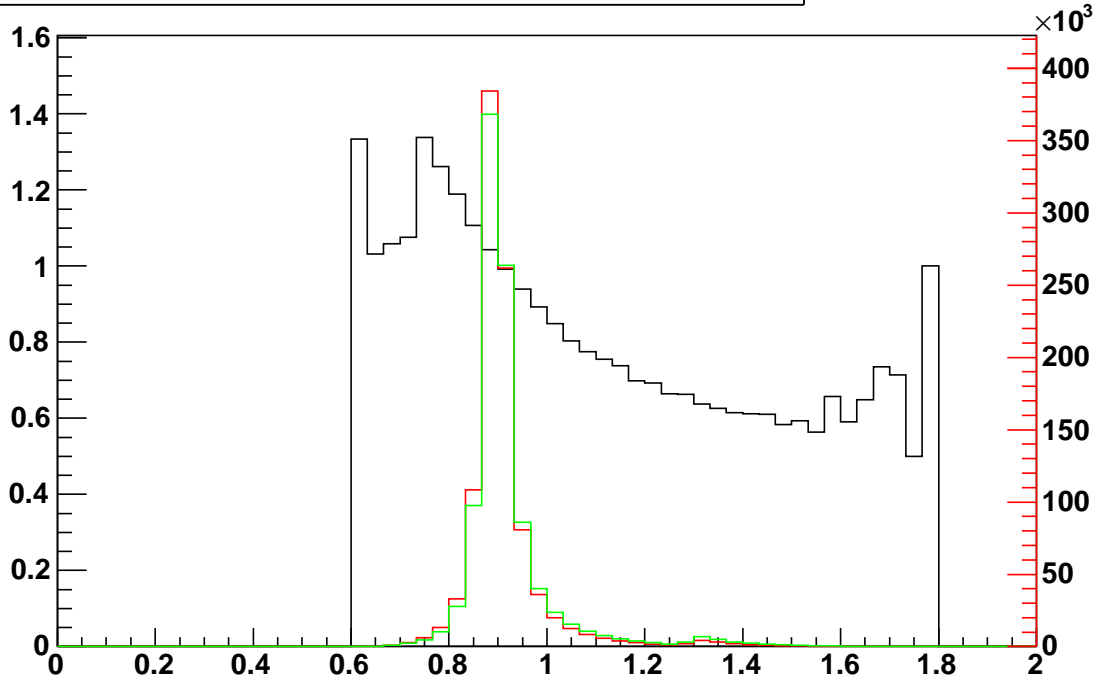


Figure 10: Normalized events distribution vs. invariant mass of  $\pi^0 K^-$  pair: no FSI case corresponds to the red (darker grey) line, for FSI the green (lighter grey) line was used. Adjustment of numerical parameters is taken into account (Shift of  $K^*$  mass, etc.). Ratio of the two histograms is given by the black one (only in this case the left side scale should be used). We have used MC-TESTER, Ref. [57], for preparation of the plot. Some of automatically generated markings are explicitly left on the plot in this case. The program, MC-TESTER, is used also for plots of our Web page [28].

Parameter	Var. name	Default	[suggested range]	Used in channel
$M_\rho$	mro	0.77554	[0.770, 0.777]	1
$M_\rho$	mro	0.775	[0.770, 0.777]	4-9,*
$M_{a_1}$	mma1	1.12	[1.00, 1.24]	5-9,*
$M_{\rho'}$	mrho1	1.453	[1.44, 1.48]	1
$M_{\rho'}$	mrho1	1.465	[1.44, 1.48]	4,5,6,*
$\Gamma_{\rho'}$	grho1	0.50155	[0.32, 0.39]	1
$\Gamma_{\rho'}$	grho1	0.4	[0.32, 0.39]	4,5,6,*
$M_{\rho''}$	mrho2	1.8105	[1.68, 1.78]	1, 4
$\Gamma_{\rho''}$	grho2	0.4178	[0.08, 0.20]	1, 4
$\gamma$	coef_ga	0.14199	[0.077, 0.099]	1, 4
$\delta$	coef_de	-0.12623	[-0.035, -0.012]	1, 4
$\phi_1$	phi_1	-0.17377	[0.5, 0.7]	1, 4
$\phi_2$	phi_2	0.27632	[0.5, 1.1]	1, 4
$M_{K^{*\pm}}$	mksp	0.89166	[0.891, 0.892]	2,3,7-9,*
$M_{K^{*0}}$	mks0	0.8961	[0.895, 0.897]	2,3,7-9,*
$M_{K^*}$	mkst	0.8953	[0.8951, 0.8955]	2,3
$M_{K^*}$	mkst	$(M_{K^{*\pm}} + M_{K^{*0}})/2$		7-9,*
$m_{K^*}$	mkst	0.94341	[0.9427, 0.9442]	2 <sup>†</sup> ,3 <sup>†</sup>
$\Gamma_{K^*}$	gamma_kst	0.0475	[0.047, 0.048]	2,3
$\gamma_{K^*}$	gamma_kst	0.06672	[0.0655, 0.0677]	2 <sup>†</sup> ,3 <sup>†</sup>
$\Gamma_{K^{*l}}$	gamma_kstpr	0.206	[0.155, 0.255]	2,3
$\gamma_{K^{*l}}$	gamma_kstpr	0.240	[0.120, 0.380]	2 <sup>†</sup> ,3 <sup>†</sup>
$M_{K^{*l}}$	mkstpr	1.307	[1.270, 1.350]	2,3
$m_{K^{*l}}$	mkstpr	1.374	[1.330, 1.450]	2 <sup>†</sup> ,3 <sup>†</sup>
$F$	fpi_rpt	0.0924	[0.0920, 0.0924]	all,*
$F_K$	fk_rpt	1.198F	[0.94F, 1.2F]	3,4
$F_V$	fv_rpt	0.18	[0.12, 0.24]	5-9,*
$G_V$	gv_rpt	$F^2/F_V$	[0.xx $F^2/F_V$ , 1.xx $F^2/F_V$ ]	5-9,*
$F_A$	fa_rpt	0.149	[0.10, 0.20]	5-9,*
$\beta_\rho$	beta_rho	-0.25	[-0.36, -0.18]	5,6*
$\gamma_{K\pi}$	gamma_rcht	-0.043	[-0.033, -0.053]	2,3
$\gamma_{K\pi}$	gamma_rcht	-0.039	[-0.023, -0.055]	2 <sup>†</sup> ,3 <sup>†</sup>
$\theta_V$	THETA	35.26°	[15°, 50°]	7,8

Table 4: Initialization parameters defined in file `new-currents/RChL-currents/value_parameter.f`: part 2, fit parameters. An educated guess for the variation of some of the resonance parameters is given. Energy units are powers of GeV. Channels identification numbers are defined in Table 6. Variables requiring rerun of pre-tabulation `new-currents/RChL-currents/tablet/a1/dalwid_tot_rho1_gauss.f` are marked with \*. The parameters corresponding to non-default currents of  $K\pi$  modes (FFKPIVEC=0) are marked with <sup>†</sup>.

Parameter	Var. name	Default	[suggested range]	Used in channel
$c_1 - c_2 + c_5$	c125	0.0		7-9
$2g_4 + g_5$	g4; g5	-0.6	[-0.64, -0.56]	7,8
$g_2$	g2	$\frac{M_V}{192\pi^2\sqrt{2}F_V}$	[-33%, +33%]	7-9
$g_1 - g_3$	g13	$\frac{-2M_V}{192\pi^2\sqrt{2}F_V}$	[-33%, +33%]	7-9
$c_1 - c_2 - c_5 + 2c_6$	c1256	$-\frac{3F_V M_V}{96\pi^2\sqrt{2}F^2}$	[-33%, +33%]	7-9
$d_3$	d3	$-\frac{M_V^2}{64\pi^2 F^2}$	[-33%, +33%]	7-9
$d_1 + 8d_2 - d_3$	d123	0.05	[-50%, +50%]	7-9
$c_1 + c_2 - 8c_3 - c_5$	c1235	0.0	[-0.25, +0.25]	7-9
$c_4$	c4	-0.07	free	7-9
$g_4$	g4	-0.72	free	7,8

Table 5: Initialization part 3: odd-intrinsic parity sector. File `new-currents/RChL-currents/value_parameter.f`. Channels identification numbers are defined in Table 6. The defaults, which follow Refs. [25, 121], are needed to reproduce our figures.

No.	Channel	Width [GeV]	Reference	In <code>new-currents/RChL-currents</code> directory channel's current: file $\rightarrow$ routine
1.	$\pi^- \pi^0$	$5.2441 \cdot 10^{-13} \pm 0.005\%$	Subs. 2.4	<code>frho_pi.f</code> $\rightarrow$ <code>CURR_PIPiO</code>
2.	$\pi^0 K^-$	$8.5810 \cdot 10^{-15} \pm 0.005\%$	Subs. 2.4	<code>fkpipl.f</code> $\rightarrow$ <code>CURR_KPiO</code>
3.	$\pi^- \bar{K}^0$	$1.6512 \cdot 10^{-14} \pm 0.006\%$	Subs. 2.4	<code>fkpipl.f</code> $\rightarrow$ <code>CURR_PiKO</code>
4.	$K^- K^0$	$2.0864 \cdot 10^{-15} \pm 0.007\%$	Subs. 2.4	<code>fk0k.f</code> $\rightarrow$ <code>CURR_KKO</code>
5.	$\pi^- \pi^- \pi^+$	$2.0800 \cdot 10^{-13} \pm 0.017\%$	Subs. 2.1	<code>f3pi_rcht.f</code> $\rightarrow$ <code>F3PI_RCHT*</code>
6.	$\pi^0 \pi^0 \pi^-$	$2.1256 \cdot 10^{-13} \pm 0.017\%$	Subs. 2.1	<code>f3pi_rcht.f</code> $\rightarrow$ <code>F3PI_RCHT*</code>
7.	$K^- \pi^- K^+$	$3.8460 \cdot 10^{-15} \pm 0.024\%$	Subs. 2.2	<code>fkmpi.f</code> $\rightarrow$ <code>FKKPi*</code>
8.	$K^0 \pi^- \bar{K}^0$	$3.5917 \cdot 10^{-15} \pm 0.024\%$	Subs. 2.2	<code>fkmpi.f</code> $\rightarrow$ <code>FKKPi*</code>
9.	$K^- \pi^0 K^0$	$2.7711 \cdot 10^{-15} \pm 0.024\%$	Subs. 2.3	<code>fk0pi0.f</code> $\rightarrow$ <code>FKKOPIO*</code>
				*The $F_i$ of formula (3).
1.	$\pi^- \pi^0$	$4.0642 \cdot 10^{-13} \pm 0.005\%$	Subs. 2.4	<code>frho_pi.f</code> $\rightarrow$ <code>CURR_PIPiO**</code>
2.	$\pi^0 K^-$	$7.4275 \cdot 10^{-15} \pm 0.005\%$	Subs. 2.4	<code>fkpipl.f</code> $\rightarrow$ <code>CURR_KPiO**</code>
3.	$\pi^- \bar{K}^0$	$1.4276 \cdot 10^{-14} \pm 0.006\%$	Subs. 2.4	<code>fkpipl.f</code> $\rightarrow$ <code>CURR_PiKO**</code>
4.	$K^- K^0$	$1.2201 \cdot 10^{-15} \pm 0.007\%$	Subs. 2.4	<code>fkpipl.f</code> $\rightarrow$ <code>CURR_KKO**</code>
				**FSI off

Table 6: Collection of numerical results to be obtained from the `demo-standalone`. Possible future extensions going beyond the published paper will be documented in this table in the paper version included with the distribution tar-ball. References to subsections may be replaced in the future by references to the forthcoming papers. Last column includes references to routines of the currents code. This table is complementary to Table 2. Results for the case when Final State Interactions (FSI) switched off with the help of `FFVEC = 0` in file `new-currents/RChL-currents/value_parameter.f` are also given, then `FFKVEC = 1` was used.

